Zero-Temperature Phase Transitions of Antiferromagnetic Ising Model of General Spin on a Triangular Lattice

Chen Zeng[a*] and Christopher L. Henley[b]
[a] *Department of Physics, Syracuse University, Syracuse, NY 13210, USA*
[b] *Department of Physics, Cornell University, Ithaca, NY 14853, USA*
(February 1, 2008)

arXiv:cond-mat/9609007v2 28 Jul 1997

We map the ground-state ensemble of antiferromagnetic Ising model of spin-S on a triangular lattice to an interface model whose entropic fluctuations are proposed to be described by an effective Gaussian free energy, which enables us to calculate the critical exponents of various operators in terms of the stiffness constant of the interface. Monte Carlo simulations for the ground-state ensemble utilizing this interfacial representation are performed to study both the dynamical and the static properties of the model. This method yields more accurate numerical results for the critical exponents. By varying the spin magnitude in the model, we find that the model exhibits three phases with a Kosterlitz-Thouless phase transition at $\frac{3}{2} < S_{KT} < 2$ and a locking phase transition at $\frac{5}{2} < S_L \leq 3$. The phase diagram at finite temperatures is also discussed.

PACS numbers: 75.10.Hk, 64.60.Fr, 68.35.Rh, 75.40.Mg

I. INTRODUCTION

Over the years it has been found that there exist many two-dimensional classical spin models, discrete and continuous alike, whose ground-state manifolds are macroscopically degenerate and, more interestingly, also exhibit critical behaviours, i.e., spin-spin correlation functions within the ground-state ensembles decay with distance as power laws. The classification of universality class for these models has always been a challenging problem [1]

An earlier example of this kind is the antiferromagnetic Ising model on the triangular lattice. The exact solution for this model by Stephenson [2] showed that although this model remains paramagnetic at nonzero temperature, its ground state is critical. Later works by Blöte *et al* revealed yet another remarkable property of the ground-state ensemble of this model, namely, it permits a Solid-on-Solid (SOS) representation in which spin fluctuations are subsequently described by the fluctuating interface in the SOS model [3]. Recent studies also demonstrated that this interfacial representation provides a valuable avenue for studying the ground-state ordering of quantum magnets [4,5] and the ground-state roughness of oriented elastic manifolds in random media [6]. Other recently studied models with critical ground states include three-state antiferromatic Potts model on the Kagomé lattice [7,8], the $O(n)$ model on the honeycomb lattice [9,10], the Four-Coloring model on the square lattice [11,12], and the square-lattice non-crossing dimer model and dimer-loop model [13]. On the other hand, some very similar models with degenerate ground states exhibit long-range order, such as the constrained 4-state Potts antiferromagnet [14].

In this article we study the ground-state properties of antiferromagnetic Ising model of general spin on a triangular lattice which also belongs to the class of models mentioned above. Recent numerical studies of this model include Monte Carlo simulations [15,16] and transfer matrix calculations [17]. Here we revisit this model by performing Monte Carlo simulations. The motivation of the present work is two-fold: (1)unlike previous simulations, we utilize the interfacial representation directly in analyzing the simulation results, for example, we compute the stiffness constant of the fluctuating interface which, in turn, yields more accurate critical exponents of various operators; and (2) we also study the dynamical properties of this model for the first time making use of the interfacial representation.

The body of the this paper is organized as follows. Section II describes the model Hamiltonian and maps it onto a spin-1 problem whose interfacial representation is then described. In Section III, we propose an effective continuum theory for the long-wavelength fluctuations of the interface. Here we also show how to relate scaling dimensions of various operators to the stiffness constant of the interface, and derive some other analytical results based on this "height representation." This allows analytical understanding of the phase diagram (Sec. IV). Details of Monte Carlo simulations and numerical results on both dynamical and static properties are presented in Section V, including a comparison of the new and old approaches to determining the exponents. As a conclusion, the paper is summarized and various possible extensions are outlined, in Section VI.

II. THE MODEL

The antiferromagnetic Ising model of spin-S on a triangular lattice can be described by the following Hamiltonian:

$$H = J \sum_{\mathbf{r}} \sum_{\mathbf{e}} s(\mathbf{r}) s(\mathbf{r}+\mathbf{e}) \tag{1}$$

where the spin variable $s(\mathbf{r})$ defined on lattice site $\mathbf{r}$ of the triangular lattice can take any value from a discrete set $[-S, -S+1, \cdots, S-1, S]$, and the sum over $\mathbf{e}$ runs over three nearest-neighbor vectors $\mathbf{e}_1$, $\mathbf{e}_2$ and $\mathbf{e}_3$ as shown in Fig. 1. Here the coupling constant J is positive describing the antiferromagnetic exchange interaction between two nearest-neighbor spins: $s(\mathbf{r})$ and $s(\mathbf{r}+\mathbf{e})$.

One important reason for interest in this model is that the $S \to \infty$ limit [18] is the same as the Ising limit of the (classical or quantum) Heisenberg antiferromagnet on the triangular lattice with Ising-like anisotropic exchange. That model was shown to exhibit a continuous classical ground state degeneracy and unusual features of the selection by fluctuations of ground states [19].

The ground-state configurations of the above model given by Eq. (1) consist of entirely of triangles on which one spin is $+S$, another is $-S$, and the third can be anything in $[-S, +S]$. Thus, if spin $s(\mathbf{r})$ takes an intermediate value $-S < s(\mathbf{r}) < S$, this forces the six surrounding spins to alternate $+S$ and $-S$; exactly which intermediate value $s(\mathbf{r})$ takes does not matter in determining whether a configuration is allowed.

A. Spin-1 mapping

Therefore, this allows us to reduce each state $\{s(\mathbf{r})\}$ to a state $\{\sigma(\mathbf{r})\}$ of a *spin-1* model, by mapping $s(\mathbf{r}) = +S$ to $\sigma(\mathbf{r}) = +1$, $s(\mathbf{r}) = -S$ to $\sigma(\mathbf{r}) = -1$, and intermediate values $-S < s(\mathbf{r}) < +S$ to $\sigma(\mathbf{r}) = 0$. In this *spin-1* representation of the model, the rules for allowed configurations are exactly the same as for the $S = 1$ model; however instead of being equal, the statistical weights have a factor $2S - 1$ for each spin with $\sigma(\mathbf{r}) = 0$. It should be noted that in the $S = 1/2$ case, $s(\mathbf{r}) = \pm 1/2$ simply maps to $\sigma(\mathbf{r}) = \pm 1$.

It can also be shown that the expectation of any polynomial in $\{s(\mathbf{r})\}$, in the ground-state ensemble of the spin-S model, can be written in terms of a similar expectation in the spin-1 model. Specifically, one must simply replace

$$s(\mathbf{r})^m \to \begin{cases} S^m \sigma(\mathbf{r}), & \text{m odd} \\ S^m[(1 - C_m(S))\sigma(\mathbf{r})^2 + C_m(S)], & \text{m even} \end{cases} \tag{2}$$

where (e.g.) $C_2(S) = \frac{1}{3}(1 - S^{-1})$. Thus there is no loss of information in this mapping. Indeed, in some sense, the extra freedom to have $s(\mathbf{r})$ vary from $-(S-1)$ to $S-1$ is trivial: once given that $s(\mathbf{r})$ and $s(\mathbf{r}')$ are intermediate spin values, there is no correlation between these values.

So we henceforth restrict ourselves to the spin-1 mapped model whose partition function for its ground-state ensemble can be written as:

$$Z = \sum_{\{\sigma(\mathbf{r})\}} (2S-1)^{n_s} \quad , \tag{3}$$

where n_s denotes the number of zero spins in a ground-state configuration $\{\sigma(\mathbf{r})\}$. By varying the weight factor continuously in the spin-1 model, it would possible to give a precise meaning to *any* real value of S, and to simulate such an ensemble. However, in this article we perform Monte Carlo simulations for an ensemble in which $2S$ takes only integer values.

The spin-1 representation could be further reduced to a spin-1/2 representation $\tilde{\sigma}(\mathbf{r})$ as described in Refs. [20,17,16]. They let

$$\tilde{\sigma}(\mathbf{r}) \equiv \sigma(\mathbf{r}) + k(\mathbf{r}) \tag{4}$$

Here $k(\mathbf{r}) = 0$ if $\sigma(\mathbf{r}) = \pm 1$ and if $\sigma(\mathbf{r}) = 0$, $k(\mathbf{r}) = +1$ or -1 according to whether the surrounding spins are $(+1, -1, +1, -1, +1, -1)$ or the reverse. Note this mapping is not invertible. The spin-1/2 representation is less satisfactory in that is arbitrarily breaks the up-down symmetry of correlation functions, but it was desirable for the transfer-matrix calculations of Lipowski *et al* [17] since it reduced the number of degrees of freedom.

B. Height mapping

We define a *microscopic*, discrete-valued height function $z(\mathbf{r})$ living on the vertex of the triangular lattice such that the step in $z(\mathbf{r})$ between adjacent vertices is a function of the adjacent spins:

$$z(\mathbf{r}+\mathbf{e}) - z(\mathbf{r}) = \frac{1}{2} + \frac{3}{2}\sigma(\mathbf{r}+\mathbf{e})\sigma(\mathbf{r}) \quad , \tag{5}$$

where $\sigma(\mathbf{r})$ is the spin-1 operator and $\mathbf{e}$ can be any of the three nearest-neighbor vectors $\mathbf{e}_{1,2,3}$. It is easy to show that the total change in height function, when traversed along any smallest loop, i.e, an elementary triangle, is zero. Therefore, $z(\mathbf{r})$ is well-defined everywhere for the ground-state configurations, but it is not well-defined in any excited state. This prescription generalizes that originally introduced by Blöte et al for the case $S = 1/2$ [3,21,22] (the prescriptions agree in that case).

This type of height mapping differs from other sorts of mapping (e.g. dualities) in a crucial way: since the spin microstates of the spin-1 model are mapped essentially one-to-one to the height microstates, it is possible to perform Monte Carlo simulations and construct configurations $z(\mathbf{r})$ after each time step. We have found that analysis of the $z(\mathbf{r})$ correlations is much more efficient for extracting critical exponents than analysis of the spin correlations directly as was done in previous Monte Carlo simulations [15].

III. HEIGHT REPRESENTATION THEORY

In this section we propose an effective continuum theory which describes the long-wavelength fluctuations of

the interface. We also demonstrate how the critical exponents of various operators are determined by the stiffness constant of the interface.

A. Effective free energy

To describe the interface in the rough phase, we must define a smooth height field $h(\mathbf{x})$ by coarse-graining the discrete field $z(\mathbf{r})$. As a first stage, on every triangular plaquette formed by sites $\mathbf{r}_1, \mathbf{r}_2, \mathbf{r}_3$, define a new discrete height

$$h(\mathbf{R}) \equiv \frac{1}{3}(z(\mathbf{r}_1) + z(\mathbf{r}_2) + z(\mathbf{r}_3)) \ , \tag{6}$$

where $\mathbf{R}$ is the center of a triangle. The possible values of the $h(\mathbf{R})$ are $\{n/2\}$, for any integer n. (For the case $S = 1/2$, the only possible values are integers.) To each of these values corresponds a *unique* ground-state spin configuration of the spin-1 model on that triangle, i.e.,

$$s(\mathbf{r}) = \Phi_s(h(\mathbf{r} + \mathbf{u}) - h_0(\mathbf{r})) \ , \tag{7}$$

where $\mathbf{u}$ is any vector from a site to the center of any adjoining triangle. The mapping is many-to-one: the function $\Phi_s(h)$ has period 6. Notice that the r.h.s. of Eq.(7) turns out to be independent of $\mathbf{u}$, but the periodic dependence on h is phase-shifted by a function $h_0(\mathbf{r})$ which takes different values on each of the three $\sqrt{3} \times \sqrt{3}$ sublattices. Essentially, we have mapped the $T = 0$ ensemble of the spin-1 problem into an equivalent interface problem. Note that, given a configuration of $\{h(\mathbf{R})\}$, each $\sigma(\mathbf{r})$ is specified (via Eq. (7)), once for each adjoining triangle. The requirement that these six values of $\sigma(\mathbf{r})$ coincide translates to a somewhat complicated set of contraints between pairs $h(\mathbf{R})$ and $h(\mathbf{R}')$ on adjoining triangles; the difference $h(\mathbf{R}) - h(\mathbf{R}')$ may be 0, $\pm 1/2$, or ± 1, but some of these are disallowed (depending on which $h()$ values are integer or half-odd-integer, and on the orientation of $\mathbf{R} - \mathbf{R}'$). The weight of each configuration is given, as in (3), by by $(2S-1)^{n_s}$.

Fig. 1 shows the $h(\mathbf{R})$ mapping explicitly where the spins $\sigma(\mathbf{r})$ take values from $\{+1, 0, -1\}$. The twelve states are arranged in a circle because the pattern repeats when $h \to h \pm 6$.

There are certain special "flat states" in which $h(\mathbf{R})$ is uniform on all triangles. Each of these is periodic with a $\sqrt{3} \times \sqrt{3}$ unit cell – in effect it is a repeat of one of the triangles in Fig. 1. We shall name these states by writing the spins on the three sublattices,"$(+,+,-)$" and "$(+,-,0)$"; here "$\pm$" stands for $\sigma = \pm 1$. It should be noted that there are two non-equivalent species of flat state corresponding to integer, and half-integer valued $h(\mathbf{R})$ respectively. They are non-equivalent in the sense that they are not related by *lattice* symmetries. One of the species that is favored by the *locking potential* (see Eq. (9) below) is what is previously called "ideal" states [11–14].

Thus we can imagine that all states can be described as domains of uniform $h(\mathbf{R})$ separated by domain walls. Finally, by coarse-graining $h(\mathbf{R})$ over distances large compared to the lattice constant, one obtains $h(\mathbf{x})$ which enters the conjectured continuum formula for the free energy, which is entropic in origin [3],

$$F(\{h(\mathbf{x})\} = \int d\mathbf{x} \left[\frac{K}{2} |\nabla h(\mathbf{x})|^2 + V(h(\mathbf{x})) \right] \ , \tag{8}$$

where K is the stiffness constant of the fluctuating interface.

A lattice shift by one lattice constant leaves the free energy invariant, but induces global shifts in height space $h(\mathbf{x}) \to h(\mathbf{x}) \pm 1$; hence the potential $V(\cdot)$ in (8) must have period one. It is typically approximated as

$$V(h) \approx h_V \cos(2\pi h). \tag{9}$$

Such a periodic potential, usually referred as the *locking term* [23], favors the heights to take their discrete values one of the two types of flat state, depending on the sign of h_V. For large S we expect $h_V < 0$, favoring the $(+,-,0)$ states, in view of the large entropy of flippable spins; it is not so sure which state is favored at smaller S, but this does not matter for the critical exponents (see Sec. III C and III D, below.

B. Fluctuations and correlation functions

In the *rough phase*, by definition, the locking term is irrelevent, and so the long-wavelength fluctations of height variable $h(\mathbf{x})$ are governed by the Gaussian term of Eq. (8):

$$F(\{h(\mathbf{x})\} = \int d\mathbf{x} \frac{K}{2} |\nabla h(\mathbf{x})|^2 = \sum_{\mathbf{q}} \frac{K}{2} \mathbf{q}^2 |h(\mathbf{q})|^2 \ , \tag{10}$$

where we have performed the Fourier transform. Hence by equipartition theorem,

$$S_h(\mathbf{q}) \equiv \langle |h(\mathbf{q})|^2 \rangle = \frac{1}{K\mathbf{q}^2} \ . \tag{11}$$

Similarly, we can also measure the *height-height difference function* in the real space as:

$$\begin{aligned} C_h(\mathbf{R}) &\equiv \frac{1}{2} \langle [h(\mathbf{R}) - h(\mathbf{0})]^2 \rangle \\ &= \frac{1}{2\pi K} \ln(\pi R/a) + ... \ \ (R \gg 1) \ , \end{aligned} \tag{12}$$

where a is the lattice spacing cutoff.

C. Scaling dimensions

Using Eq. (12), we can compute the scaling dimension x_O of any *local* operator $O(\mathbf{r})$, which is defined as in the correlation function,

$$\langle O^*(\mathbf{r})O(\mathbf{0})\rangle \sim r^{-2x_O} \quad . \tag{13}$$

By local operator, we mean that $O(\mathbf{r})$ is a local function of spin operators in the vicinity of $\mathbf{r}$. Now, the same spin configuration is recovered when the height variable $h(\mathbf{R})$ is increased by 6. [24] Thus any local operator $O(\mathbf{r})$ is also a periodic function in the height space, and can consequently be expanded as a Fourier series:

$$O(\mathbf{r}) = \sum_G O_G e^{iGh(\mathbf{r})} \sim e^{iG_O h(\mathbf{r})} \quad , \tag{14}$$

where G runs over height-space reciprocal-lattice vectors (i.e. multiples of $2\pi/6$). The last step of simplification in (14) follows because the scaling dimension x_O of the operator $O(\mathbf{r})$ is determined by the leading relevant operator in the above expansion, i.e., G_O is the smallest G with nonzero coefficient in the sum. Inserting Eq. (14) into Eq. (13) and making use of Eq. (12), we obtain the following:

$$\begin{aligned}\langle O^*(\mathbf{r})O(\mathbf{0})\rangle &= \langle e^{-iG_O h(\mathbf{r})} e^{iG_O h(\mathbf{0})}\rangle \\ &= e^{-G_O^2 C_h(\mathbf{r})} \sim r^{-\eta_O} \quad .\end{aligned} \tag{15}$$

Therefore, the critical exponent η_O associated with the operator $O(\mathbf{r})$ is given by:

$$\eta_O \equiv 2x_O = \frac{1}{2\pi K}|G_O|^2 \quad . \tag{16}$$

D. Definition of operators

In this paper, besides the usual spin operator $\sigma(\mathbf{r})$, we also study the bond-energy operator $E(\mathbf{r}+\mathbf{e}/2)$ for the reason that will become clear in the next section:

$$E(\mathbf{r}+\mathbf{e}/2) = \frac{1}{2} + \frac{3}{2}\sigma(\mathbf{r}+\mathbf{e})\sigma(\mathbf{r}) \quad , \tag{17}$$

where $\mathbf{e}$ denotes one of the three nearest-neighbor vectors as before.

As discussed already, the spin operator on a given site has a periodicity of 6 in the height space, from which a simple inspection shows that the bond-energy operator is also periodic in the height space with a periodicity of 3. Therefore, the reciprocal lattice vectors of the most relevant operator in the Fourier expansion in Eq. (14) are

$$G_\sigma = \frac{2\pi}{6}, \quad G_E = \frac{2\pi}{3} \quad , \tag{18}$$

for spin and bond-energy operators respectively.

If a magnetic field is implemented by adding a term $-H\sum_{\mathbf{r}}\sigma(\mathbf{r})$ to the Hamiltonian, then our dimensionless uniform "magnetic field" is defined by $H' \equiv H/T$. The exponents associated with H' (and with the uniform magnetic susceptibility), are easily related to the correlation exponents of the uniform magnetization operator,

$$M(\mathbf{R}) = \frac{1}{3}(\sigma(\mathbf{r}_1)+\sigma(\mathbf{r}_2)+\sigma(\mathbf{r}_3)) \quad , \tag{19}$$

where $\mathbf{R}$ is the center of a triangle formed by sites $\mathbf{r}_1, \mathbf{r}_2, \mathbf{r}_3$. A simple inspection of Fig. 1 shows that such an operator has a periodicity of 2 in the height space, thus yielding:

$$G_M = \frac{2\pi}{2} \quad . \tag{20}$$

E. Zone-corner singularities

Observe that the microscopic height variable $z(\mathbf{r})$ in any flat state is not uniform but is rapidly modulated with the wave vector $\mathbf{Q} = \frac{4\pi}{3}(1,0)$. The amplitude of modulation itself is a periodic function of the *coarse-grained* height field $h(\mathbf{x})$ which in turn implies that the correlation function decays with distance as a power-law, and consequently that its structure factor has a power-law singularity at $\mathbf{Q}$.

Such a zone-corner singularity is also directly connected to the singularity in the structure factor of the bond-energy operator. To see this, recall that there is a linear relation between the microscopic height variables and the bond-energy operator given by Eqs. (5) and (17), i.e.,

$$E(\mathbf{r}+\frac{\mathbf{e}}{2}) = z(\mathbf{r}+\mathbf{e}) - z(\mathbf{r}) \quad . \tag{21}$$

Then it is interesting to note that the Fourier transform $E_{\mathbf{e}}(\mathbf{q})$ of bond-energy operator given above turns out to be

$$\begin{aligned}E_{\mathbf{e}}(\mathbf{q}) &\equiv N^{-1/2}\sum_{\mathbf{r}} e^{i\mathbf{q}\cdot(\mathbf{r}+\frac{\mathbf{e}}{2})} E(\mathbf{r}+\frac{\mathbf{e}}{2}) \\ &= -2i\sin(\frac{1}{2}\mathbf{q}\cdot\mathbf{e})z(\mathbf{q}) \quad .\end{aligned} \tag{22}$$

In other words, as a byproduct of measuring $\langle|z(\mathbf{q})|^2\rangle$, we have at the same time measured the structure factor of, say, the bond-energy operator of the same orientation specified by the nearest-neighbor vector $\mathbf{e}$:

$$S_E(\mathbf{q}) \sim \langle|E_{\mathbf{e}}(\mathbf{q})|^2\rangle = 4\sin^2(\frac{1}{2}\mathbf{q}\cdot\mathbf{e})\langle|z(\mathbf{q})|^2\rangle \quad . \tag{23}$$

We will utilize this relation in Sec. V D to extract the exponent of bond-energy operator from the Monte Carlo simulations.

F. Exact solution for $S = 1/2$

The $S = 1/2$ triangular Ising antiferromagnet is exactly soluble, by the same techniques which solve the ferromagnetic two-dimensional Ising model, and was immediately recognized to have critical behavior as $T \to 0$. The spin and energy correlation functions were computed exactly by Stephenson; it transpires that $\eta_\sigma = 1/2$ and $\eta_E = 2$ exactly, implying through the arguments of Blöte et al (see Sec. III C and III D) that the effective stiffness in Eq. (10) is $K = \pi/9$ exactly. The exponents implied by the interface scenario [3] – in particular, the magnetic field exponent η_M – are fully confirmed by numerical transfer-matrix computations. [25]

The Coulomb gas picture of Kondev *et al* [26], wherein the $S = 1/2$ triangular Ising antiferromagnet is viewed as a fully-packed loop model [9] with fugacity 1, also predicts the exact exponents.

IV. PHASE DIAGRAM

In this section, we collect some consequences of the height representation for the phase diagram and the nature of the various phases within it. [28]

A. Kosterlitz-Thouless and locking transitions

The locking potential $V(\cdot)$ in (8) favors the flat states. In view of (9), its leading reciprocal-lattice vector is $G_V = 2\pi$, corresponding to a scaling index $x_V = |G_V|^2/\pi K = \pi/K$ for the corresponding conjugate field h_V. It is well known that if $2 - x_V > 0$, then h_V becomes relevant (under renormalization and the interface locks into one of the flat states. [23] Since K grows monotonically with S, such a locking transition occurs at a critical S_L where $K_L = \pi/2 = 1.57079...$ [3,17]. In this "smooth" phase, any spin operator $O(\mathbf{r})$ has long-range order, by arguments as in Sec. III C.

B. Fluctuations in smooth phase

One of our aims in this paper was to pinpoint the locking transition S_L, which demands that we have a criterion to distinguish these phases. We must supplement Eq. (11), which shows the expected qualitative behavior of height fluctuations $\langle |h(\mathbf{q})|^2 \rangle$ in the rough phase, with a parallel understanding of the smooth phase.

In the smooth state, the symmetry (of height shifts) is broken and a fully equilibrated system has long-range order, such that $\langle h(\mathbf{x}) \rangle$ is well defined and uniform throughout the system. Fluctuations around this height, then, have at most short-range (exponentially decaying) correlations. Thus we expect them to have a spatial "white noise" spectrum:

$$\langle |h(\mathbf{q})|^2 \rangle \sim \text{const} \tag{24}$$

for small $\mathbf{q}$.

A phase with "hidden" order was suggested by Lipowski and Horiguchi [17,20]. Numerical transfer-matrix calculations [17] using the spin-1/2 representation indicated $0 < \eta_\sigma < 1/9$ for $2S > 6$, which is impossible if the spin correlations are derived from height fluctuations, [3] as we reviewed in Sec. III. An exotic phase to reconcile these facts was to postulate a phase in which the interface was smooth and $\langle \tilde{\sigma}(\mathbf{r}) \rangle \neq 0$, yet for the real spins $\langle \sigma(\mathbf{r}) \rangle = 0$ as suggested by spin correlation measurements.

What does this imply for our height variable $h(\mathbf{R})$, which has a one-to-one correspondence with the real spin configuration $\{\sigma(\mathbf{r})\}$? If the interface is smooth, then the probability distribution of height values on a given plaquette, $P(h(\mathbf{R}))$, is well defined. In order to "hide" the order, it is necessary that $P(h)$ correspond to zero expectations of the spins. Now, reversing $s(\mathbf{r})$ on all three sites in the plaquette requires $h \to h \pm 3$, as seen from Fig. 1. One can convince oneself that, to have ensemble average $\langle \sigma(\mathbf{r}) \rangle = 0$, the distribution $P(h)$ must be at least as broad as $\frac{1}{2}\delta(h-h_1)+\frac{1}{2}\delta(h-h_2)$, with $h_1 - h_2 = \langle h \rangle \pm 3$, implying the bound

$$Var[h(\mathbf{R})] \equiv \langle h(\mathbf{R})^2 \rangle - \langle h(\mathbf{R}) \rangle^2 \geq (3/2)^2. \tag{25}$$

C. Finite temperature behavior

At $T > 0$, plaquettes with non-minimal energy are present and they correspond to vortices in the function $h(\mathbf{x})$. Thus, unfortunately, the height approach of analyzing simulations more or less breaks down. Nevertheless, one can still predict the $T > 0$ phase diagram from knowledge of the $T = 0$ stiffness constant derived from our simulations. The shape of this phase diagram has already been explained in Ref. [17]; here we note some additional interesting behaviors which can be predicted (following Ref. [3](b)) using the exponents associated with vortices.

The other exponents in Kosterlitz-Thouless (KT) theory are associated with elementary defects (often called vortices). Indeed, it is easy to check (in this system) that the excess energy of a non-ground-state plaquette is directly proportional to its vortex charge (a Burgers vector in height-space), so the effect of nonzero temperature is simply to make the vortex fugacity nonzero. The vortex exponent is $\eta_v = 1/\eta_\sigma$, so as usual the vortex fugacity becomes relevant and defects unbind, destroying the critical state, at the KT transition defined by a spin

exponent taking the critical value $\eta_\sigma = 1/4$. If $\eta_\sigma > 1/4$ at zero temperature, i.e. $K < K_{KT} \equiv 2\pi/9 = 0.69813...$, then defects unbind as soon as $T > 0$. Thus a zero-temperature KT transition occurs at S_{KT} defined by $K = K_{KT}$. [17]

Ref. [17] did not, however, address the critical exponents of the correlation length $\xi(T)$ and the specific heat $C(T)$ as a function of temperature, which are also controlled by vortex exponents. Naively, if the energy cost creating one vortex is E_c, and if the minimum excitation is a vortex pair, then one would expect the low-temperature specific heat to behave as $C(T) \sim \exp(-2E_c/T)$ and at $S = 1/2$ this is indeed true [27]. However, the renormalization group [3] shows the singular specific heat behaves as

$$f(T) \sim y(T)^{4/(4-\eta_v)} \tag{26}$$

where $y(T) = \exp(-E_c/T)$ is the vortex fugacity; consequently when $\eta_v < 2$, the true behavior is

$$C(T) \sim \exp(-2E_1/T) \tag{27}$$

with $E_1 = 2E_c/(4 - \eta_v) < E_c$. (Physically, part of the excitation energy is cancelled by the large entropy due to the many places where the vortex pair could be placed.) This behavior has been observed in the 3-state Potts antiferromagnet on the Kagomé lattice [7], and should occur in the present system for all $S > 1/2$.

D. Finite magnetic field

It is interesting to consider the effect of a nonzero magnetic field H'. It is known already that at $S = 1/2$, [3] such a field is an irrelevant perturbation, so that the system remains in a critical state, yet at sufficiently large H it undergoes a locking into a smooth phase, [25] approximated by any of the three symmetry-equivalent flat states of type "$(+,+,-)$" with magnetization $S/3$

As also already noted [17], there is a critical value S_{cH} defined by $\eta_\sigma(S_{cH}) = 4/9$, beyond which $\eta_M = 9\eta_\sigma < 4$ so that the system locks into long-range order as soon as H' is turned on. Within this regime, there are still two subregimes with different behavior of $M(h)$ near $h = 0$. For $2 < \eta_M < 4$, the initial slope is zero, i.e., the susceptibility is not divergent; when $\eta_M < 2$, as occurs for $S \geq 2$, there is a divergent susceptibility and correspondingly there should be a singularity at $\mathbf{q} = 0$ in the spin structure factor $\langle|\sigma(\mathbf{q})|^2\rangle$.

What do we expect in the locked phase at $S > S_L$? Here the difference between the two kinds of flat states becomes crucial. The H' field favors the $(+,+,-)$ type of flat state, but entropy favors the $(+,-,0)$ type of flat state. Thus we expect a transition to the $(+,+,-)$ state only at a nonzero critical field H'_c. On reducing H' through H'_c, a twofold symmetry breaking occurs, in which one of the + sublattices becomes the 0 (disordered) sublattice; hence, this transition should be in the Ising universality class. Presumably the line $H'_c(S)$ meets the $H' = 0$ axis at $S = S_L$. There must also be line of locking transitions $S_{cH}(H')$, which terminates on the $H' = 0$ axis at S_{cH}.

For $S = 1/2$, the effect of the magnetic field was confirmed numerically in Ref. [25].

V. MONTE CARLO SIMULATIONS AND RESULTS

In this section we describe the implementation details of Monte Carlo simulations performed for spin-1 model in which $2S$ takes only integer values from 1 to 8. We then present numerical results for the relaxation times of slow modes in the Monte Carlo dynamics. Two different methods of compute the critical exponents of the spin, bond-energy, and uniform-magnetization operators are described in different sub-sections: one in terms of the extrapolated stiffness constants of the interface and the other in terms of the singularities of the corrsponding structure factors.

A. Details of Monte Carlo Simulations

A spin is called *flippable* if its six surrounding nearest-neighbor spins alternate between +1 and −1. Clearly, changing the value of this flippable spin results in another new spin configuration in the ground-state ensemble, provided that we start with a spin configuration in the ensemble. Moreover, such an update maintains the global tilt of the interface due to the *local* nature of this update. This update will be used as our Monte Carlo update in this paper. Two slightly different cases arise for different values of $2S$: (1) for $2S = 1$, the local update is precisely equivalent to a spin flip i.e., $\sigma(\mathbf{r}) \to -\sigma(\mathbf{r})$ due to the absence of zero spin; and (2) for all other values of $2S$, a random choice must be made in the local update: for example, $\sigma(\mathbf{r}) = 0 \to \sigma(\mathbf{r}) = 1$ or -1. (Recall S denotes the spin magnitude of the original model.)

Let n_s and n_f denote the number of zero-spins and flippable spins of configuration ϕ. If an attempted single-spin update for ϕ results in a new configuration ϕ' with n'_s and n'_f, then the transition probability W in accordance with the detailed balance principle is:

$$W = W_0 \cdot min\{1, \frac{n_f}{n'_f}\} \cdot min\{1, (2S-1)^{n'_s - n_s}\} \ , \tag{28}$$

where W_0 denotes the *bare* transition probability: $W_0 = \frac{1}{n_f}$ for $2S = 1$, and $W_0 = \frac{1}{2n_f}$ for $2S \geq 2$ which reflects the random choice to be made in the local update as discussed above. With the transition probability given in

Eq. (28), it is straightforward to show that the detailed balance principle is satisfied, i.e., $P(\phi)W(\phi \to \phi') = P(\phi')W(\phi' \to \phi)$, where $P(\phi)$ denotes the probability for configuration ϕ to occur and $P(\phi) \sim (2S-1)^{n_s}$ since each spin configuration in the original spin-S model has equal probability to occur. Note also that $n_f/n'_f = 1+O(1/N)$ for large N, so this rule is important only because of the finite system size.

To implement in practice the transition probability given above, we randomly select a site out of a list of the n_f flippable sites, and randomly update this spin to one of the two possible new spin values if $2S \geq 2$ or simply flip this spin if $2S = 1$. The total numbers of zero spins n'_s and flippable spins n'_f in the resulting configuration are then computed. This update is subsequently accepted with a probability: $min\{1, n_f/n'_f\} \cdot min\{1, (2S-1)^{n'_s - n_s}\}$. A practical implementation of the transition probability given in Eq. (28) is thus achieved.

Throughout this paper, a unit time or one Monte Carlo Sweep (MSC) is defined such that there are N_s attempts of updating within this unit of time (or one attempt per spin on average). Here N_s denotes the total number of spins in the simulation cell. The simulation cell always contains $N_s = 72 \times 72$ spins in this paper unless explicitly mentioned otherwise. Periodic boundary conditions are adopted. Since we always start with a flat state, the simulations are thus performed in the sector with a zero global tilt of the interface.

B. Dynamical scaling: the relaxation time $\tau_{\mathbf{q}}$

We now discuss the correlations between the configurations generated sequentially in the Monte Carlo simulations by studying the relaxation time of the slow modes in the model, namely, the Fourier modes $h_{\mathbf{q}}$ which play the role of an order parameter [5]. The linear-response dynamics of such a mode is usually formulated as a Langevin equation,

$$\frac{dh(\mathbf{x},t)}{dt} = -\Gamma \frac{\delta F(\{h(\mathbf{x})\})}{\delta h(\mathbf{x})} + \xi(\mathbf{x},t) \ , \tag{29}$$

where Γ is the dissipation constant, and the static free energy functional $F(\{h(\mathbf{x})\})$ is given by Eq. (8). Here $\xi(\mathbf{x},t)$ is a stochastic noise generated in the Markov chain of Monte Carlo simulations. As it is expected that the correlation time of the slow mode under consideration is much longer than that of the noise, and since the update steps are local and independent, it is proper to model $\xi(\mathbf{x},t)$ as Gaussian noise, uncorrelated in space or time:

$$\langle \xi(\mathbf{x},t)\xi(\mathbf{x}',t')\rangle = 2\Gamma\delta(\mathbf{x}-\mathbf{x}')\delta(t-t') \ , \tag{30}$$

in which the choice of 2Γ ensures that the steady-state of the interface under the Langevin equation (29) agrees with its equilibrium state under the free energy (8).

This linear stochastic differential equation can be solved easily by performing Fourier transform. Eq. (29) thus reduces to

$$\frac{dh(\mathbf{q},t)}{dt} = -\Gamma K|\mathbf{q}|^2 h(\mathbf{q},t) + \xi(\mathbf{q},t) \ , \tag{31}$$

which implies an exponentially decaying correlation function of $\langle h^*(\mathbf{q},t)h(\mathbf{q},0)\rangle \sim e^{-t/\tau_{\mathbf{q}}}$ with the relaxation time $\tau_{\mathbf{q}}$ given by

$$\tau_{\mathbf{q}} = \frac{1}{\Gamma K}|\mathbf{q}|^{-2} \ . \tag{32}$$

Therefore, the dynamical scaling exponent for the Monte Carlo dynamics, defined by $\tau_{\mathbf{q}} \sim |\mathbf{q}|^{-z}$, is always $z = 2$ in the rough phase.

To check this prediction on the dynamical scaling exponent in practice where the above continuum theory is regularized on a lattice, we compute the following auto-correlation function $C(\mathbf{q},t)$ of the *microscopic* height variable $z(\mathbf{q})$:

$$C(\mathbf{q},t) = \frac{\langle z^*(\mathbf{q},0)z(\mathbf{q},t)\rangle - |\langle z(\mathbf{q},0)\rangle|^2}{\langle z^*(\mathbf{q},0)z(\mathbf{q},0)\rangle - |\langle z(\mathbf{q},0)\rangle|^2} \ , \tag{33}$$

Here $\langle\rangle$ stands for the dynamical average, and the time t is measured in unit of MCS. For each interger-valued $2S = 1, 2, ..., 8$, we perform 10^5 MCS's with a flat initial configuration and compute the auto-correlation functions upto $t \leq 50$ for modes that correspond to the five smallest $|\mathbf{q}|^2$ values. In Fig. 2, we display the results so obtained for $2S = 1$. Other cases of $2S$ are found to have very similar features. It is clear from Fig. 2 that $\log_{10} C(\mathbf{q},t)$ can be fitted very well by $a - t/\tau_{\mathbf{q}}$ where a and the relaxation time $\tau_{\mathbf{q}}$ are the fitting parameters. In other words, the relaxation is strictly exponential in all cases. Note that we used a cutoff $t = 10$ in our fitting. The same fitting procedure is carried out for other cases of $2S$.

The final results of the relaxation time $\tau_{\mathbf{q}}$ as a function of $|\mathbf{q}|^2$ for $2S = 1, ..., 6$ are shown in Fig. 3; and for $2S = 6, 7, 8$ as an insert. The fact that $\tau_{\mathbf{q}}$ scales as $|\mathbf{q}|^2$ for $2S = 1, ..., 5$ as indicated by the fitting in Fig. 3 thus shows that the ground-state ensembles for $2S = 1, ..., 5$ are in the rough phase. On the other hand, it is indeed clear from the insert that for $2S = 7$ and 8, $\tau_{\mathbf{q}}$ curves downward as $|\mathbf{q}|^2 \to 0$ which is in sharp constrast to those of $2S = 1, ..., 5$. From this, we conclude that ground-state ensembles for $2S = 7$ and 8 are in the flat phase. As for $2S = 6$, it is not conclusive from the data available whether $\tau_{\mathbf{q}}$ scales as $|\mathbf{q}|^2$ or curves downward as $|\mathbf{q}|^2 \to 0$. Nonetheless, the fact that the relaxation time of the slowest mode for $2S = 6$ is longer than for any smaller *or larger* value of S, suggests that $2S = 6$ is very close to the locking transition. Further support for this phase diagram is also obtained by explicit calculations of stiffness constants and critical exponents which is discussed in the next section.

C. Stiffness constants and critical exponents

As implied by Sec. III B , the stiffness constant of the fluctuating interface can be directly measured by studying the long-wavelength fluctuations of the height variables, i.e., their structure factor as given by Eq. (11). It should be noted that concerning the task of calculating the Fourier components $h(\mathbf{q})$ in Eq. (11), it can be replaced by the approximation in terms of the *microscopic* height variables $z(\mathbf{q})$ given by

$$h(\mathbf{q}) \approx z(\mathbf{q}) \equiv \frac{w_0}{\sqrt{N_s}} \sum_{\mathbf{r}} e^{-i\mathbf{q}\mathbf{r}} z(\mathbf{r}) \ , \tag{34}$$

where $\mathbf{r}$ labels a lattice site of the finite triangular lattice of total N_s lattice sites used in the simulation. Here $w_0 = \sqrt{3}/2$ is the *weight* of a lattice site, i.e., the area of its Voronoi region, which is introduced so that the *microscopic* height variable $z(\mathbf{q})$ coincides with the *coarse-grained* height variable $h(\mathbf{q})$ in the long-wavelength limit ($\mathbf{q} \to 0$). But unlike $h(\mathbf{q})$, $z(\mathbf{q})$ still contains features such as zone-corner singularities discussed in Sec. III E that are only manifested in miscroscopic height variables.

Starting with a flat state, we perform 2×10^3 MCS's as the equilibrium time; subsequent measurements of physical quantities are carried out at intervals of 20 MCS's. This separation is a compromise between the correlation times of small $\mathbf{q}$ modes and of larger $\mathbf{q}$ modes, which are respectively much longer and somewhat shorter than 20 MCS – see Fig. 2. Each run consisted of 8×10^5 MCS, i.e. 4×10^4 measurements were taken; these were subdivided into 20 independent groups for the purpose of estimating statistical errors. The same procedure is used for all $2S = 1, 2, ..., 8$ reported in this paper.

In Fig. 4, we plot $\langle |z(\mathbf{q})|^2 \rangle^{-1}$ vs. $\mathbf{q}^2$ for $2S = 1$, including all $\mathbf{q}$ in the first Brillouin zone. From the plot, we observe that $\langle |z(\mathbf{q})|^2 \rangle^{-1}$ is remarkably isotropic up to about $\mathbf{q}^2 \sim 1.5$. This comes about because of the 6-fold rotational symmetry of the triangular lattice which ensures that *anisotropy* occurs only in q^6 and higher order terms, assuming that the function is analytic. This is in constrast to other models defined on the square lattice where anisotropy already sets in at the order of q^4 [13,10]. The lower envelope of the data points in Fig. 4 corresponds to the line of $q_y = 0$ in the q-vector space. Other cases of $2S$ are found to have very similar features as illustated in the insert of Fig. 4 where we plot the lower envelope for all $2S = 1, 2, ..., 8$. The structure factor of the height variables appears to diverge in the long-wavelength limit $|\mathbf{q}|^2 \to 0$ for all S values, even for the largest S values. (In the latter case, however, we believe one would see the plot asymptote to a constant value, in a sufficiently large system; see below.)

Two other interesting features of the structure factor are also revealed in the insert in Fig. 4: (1) for $2S \geq 2$, it appears to indicate yet another singularity at the zone corner $\mathbf{q} \to \mathbf{Q} \equiv \frac{4\pi}{3}(1, 0)$ in the thermodynamic limit $N_s \to \infty$; and (2) for $2S = 1$, it approaches a constant instead. As already discussed in Sec. III E, the appearance of zone-corner singularities is expected, the precise nature of such singularities, however, is discussed in the next section. In the remaining of this section, we analyze the zone-center singularity to check if height variables behave as required by Eq. (11) for the rough phase and consequently extract the stiffness constants.

To further study the nature of zone-center singularity in terms of how $\langle |z(\mathbf{q})|^2 \rangle$ scales as a function of $\mathbf{q}^2$ in the long-wavelength limit, we show the log-log plot of $\langle |z(\mathbf{q})|^2 \rangle^{-1}$ vs. $\mathbf{q}^2$ for $2S = 1, ..., 8$ in Fig. 5. Comparing the simulation results for different systems sizes of $L = 36$, 48 and and 72, we notice that data are well converged down to accessible small $\mathbf{q}$ vectors – except for the case of $2S = 6$ and 7, where the finite size effect is still discernible. This is, of course, consistent with the fact that $2S = 6$ and 7 are close to the locking transition where the correlation length diverges; it is interesting, however, to notice that their finite-size trends are different. In the case $2S = 6$, the data plot for $L = 72$ curves upwards less than that for $L = 48$, while in the case $2S = 7$, the $L = 72$ data show *more* upwards curvature than the $L = 48$ data.

By fitting $\langle |z(\mathbf{q})|^2 \rangle^{-1}$ to a function $q^{2\alpha}$ with α being the fitting parameter, we obtain, using the data of system size $L = 72$ and a cutoff $\mathbf{q}^2 \leq 0.5$, the exponent $\alpha = 0.990(1), 0.988(1), 0.986(2), 0.984(2), 0.974(2)$ and $0.935(1)$ respectively for $2S = 1, 2, 3, 4, 5$, and 6. Apart from the case of $2S = 6$, these values agree with $\alpha = 1$ as in the predicted $\mathbf{q}^{-2}$ power-law singularity of the structure factor in the rough phase, Eq. (11). As for $2S = 7$ and 8, $\langle |z(\mathbf{q})|^2 \rangle^{-1}$ clearly deviates from a power-law scaling and instead curves upwards to level off, which indicates that models with $2S = 7$ and 8 are in the smooth phases where $\langle |z(\mathbf{q})|^2 \rangle$ remains finite as $\mathbf{q} \to 0$, as discussed in Sec. IV B. This conclusion is in excellent agreement with that inferred from dynamical scaling analysis presented in Sec. V B.

It should be noted that in Fig. 5, as a general procedure adopted throughout this paper in extracting numerical values of some physical quantities, we have averaged the data corresponding to the same magnitude of $|\mathbf{q}|^2$ to further reduce the effect due to statistical errors. The relative statistical error on each individual data point $\langle |z(\mathbf{q})|^2 \rangle$ of small $\mathbf{q}$, which is measured directly from the variance among the 20 groups, is found to range from 1% to 3%. This is indeed consistent with the estimates of such relative errors from the relaxation times of the slowest modes of models with different values of $2S$ already given in Sec. V B. It is perhaps also worth noting that another good check on the statistical errors on each data point is to compare the values of $\langle |z(\mathbf{q})|^2 \rangle$ for three $\mathbf{q}$ vectors which are related by 120° rotations in reciprocal space, which ought to be equal by symmetry. For

example, in the case of $2S = 1$, the values of $\langle|z(\mathbf{q})|^2\rangle$ for the three $\mathbf{q}$ vectors of the same smallest magnitude $\mathbf{q}^2 = 0.0101539$ of system size $L = 72$ are, respectively, 285.551, 280.528, and 280.566, from which one thus also obtain the relative error of about 1%. This observation therefore motivates the averaging procedure used in this paper.

The stiffness constants can be subsequently determined by fitting $\mathbf{q}^{-2}\langle|z(\mathbf{q})|^2\rangle^{-1}$ to the function $K + C_1\mathbf{q}^2$ for the isotropic part of the data in which the stiffness constant K and C_1 are the fitting parameters. The final fitting on the averaged data is shown in Fig. 6 where we used a cutoff $\mathbf{q}^2 \leq 0.5$ in the fitting. We also tried other different cutoffs of $\mathbf{q}^2 \leq 0.1$ and $\mathbf{q}^2 \leq 1.0$, and found as expected that the stiffness is not sensitive to the value of cutoff as long as it falls into the isotropic part of the data. For example, we obtain, in the case of $2S = 1$, $K = 0.3488 \pm 0.0022, 0.3490 \pm 0.0008$, and 0.3488 ± 0.0006 for cutoff $\mathbf{q}^2 \leq 0.1, 0.5$, and 1.0 respectively. Therefore, taking into account of the uncertainty introduced due to the cutoff, our final estimate for the stiffness constant is then $K = 0.349 \pm 0.001$ which is in excellent agreement with the exact value $K_{\rm exact} = 0.349065....$ Similar procedure is carried out for other cases of $2S$ and the results are tabulated in Table I. In the same table, we also give the value for the critical exponents of spin, bond-energy and uniform magnetization operators which are obtained straightforwardly according to Eqs. (16), (18) and (20). The agreement of our $\eta_\sigma^{(K)}$ values with the "η_σ" values from transfer-matrix eigenvalues (see Table I of Ref. [17], is quite close and becomes better as S grows (until $2S = 6$.)

As already discussed in Sec. IV C, a Kosterlitz-Thouless (KT) transition occurs at a critical value S_{KT} where $\eta_\sigma = 1/4$, such that for $S > S_{KT}$ algebraic correlations persist even at small finite temperatures. It is clear from our data that $S_{KT} > 3/2$.

As for $2S = 6$, the value of $\mathbf{q}^{-2}\langle|z(\mathbf{q})|^2\rangle^{-1} = 1.75 \pm 0.06$ at the smallest nonzero $\mathbf{q}^2 = 0.010153$ is already larger than $K_L = \pi/2 = 1.57079$. That is, even if the system may have a "rough" behavior at the length scales probed in the simulation, the stiffness constant is such that the locking potential is relevant and must dominates at sufficiently large length scales, as discussed in Sec. IV A. A similar observation has already been used to argue that the constrained Potts antiferromagnet is in a smooth phase [14]. This fact together with the poor fitting using the formula suitable for the rough phase (see the top curve of Fig. 6) leave us little choice but to conclude that the ground-state ensemble for $2S = 6$ also falls into the smooth phase, or possibly is exactly at the locking transition.

Just as the finite-size effect for $2S = 6$ was severe both for the spin-spin correlations (measured via Monte Carlo [15,16]) and also in spin-operator eigenvalues (measured via tranfer-matrix, [17]) we similarly find it is severe for height fluctuations. However, in view of the exponential relationship between the exponents and the stiffness constant, the latter measurements are much more decisive as to the true phase of the system.

To sum up, based on the analysis on the nature of the singularity in the height structure factor at the long-wavelength limit and the numerical results on the stiffness constants, we thus conclude that the model exhibits three phases with a KT phase transition at $\frac{3}{2} < S_{KT} < 2$ and a locking phase transition at $\frac{5}{2} < S_L \leq 3$.

D. Structure factor and zone-corner singularity

Another more traditional approach [15] in calculating the critical exponents of various operators is to compute the corresponding structure factors and analyze the power-law singularities at the appropriate ordering wave vectors. Namely, if the correlation function of an operator O decays with distance as power-law (thus critical)

$$\langle O(\mathbf{r})O(\mathbf{0})\rangle \sim \frac{e^{i\mathbf{Q}\cdot\mathbf{r}}}{r^{\eta_O}} \ , \tag{35}$$

then its structure factor near the ordering vector $\mathbf{Q}$ shows a power-law singularity

$$S_O(\mathbf{q} = \mathbf{Q} + \mathbf{k}) \sim \mathbf{k}^{2(x_O-1)} \ , \tag{36}$$

from which the critical exponent $\eta_O \equiv 2x_O$ can be numerically extracted. Here in this section, we adopt this approach to calculate the critical exponents of spin, bond-energy, and uniform-magnetization operators so as to compare with those obtained from the stiffness constant.

As given by Eq. (23), $S_E(\mathbf{q} = \mathbf{Q} + \mathbf{k}) \sim \langle|z(\mathbf{q} = \mathbf{Q} + \mathbf{k})|^2\rangle$. Here $\mathbf{Q} = \frac{4\pi}{3}(1, 0)$ is the ordering vector of the bond-energy operator. Therefore the interesting feature of structure factor of height variables, namely, the appearance of zone-corner singularity as shown in Fig. 4, is not only expected but also very useful in extracting the critical exponent η_E.

Of course, such a zone-corner singularity can also be understood within the framework of interfacial representation, as in Sec. III, particularly Subsec. III E. (Similar zone-corner singularities have been studied in Refs. [11] and [13].) Finally, according to the exact result $\eta_E = 2$ ($x_E = 1$) in the case of $2S = 1$, i.e., $S_E(\mathbf{q} = \mathbf{Q} + \mathbf{k}) \sim \mathbf{k}^{2(x_E-1)} \to const.$, the puzzling absence of the zone-corner singularity for $2S = 1$ as shown in Fig. 4 is also resolved.

In Fig. 7, we plot $\log_{10} S_E(\mathbf{q})$ vs. $\log_{10}|\mathbf{q} - \mathbf{Q}|^2$ where we have averaged data points with the same magnitude of $|\mathbf{q} - \mathbf{Q}|^2$. Fitting $S_E(\mathbf{q})$ to the function $|\mathbf{q} - \mathbf{Q}|^{2(x_E-1)}(C_1 + C_2|\mathbf{q} - \mathbf{Q}|)$ where x_E, C_1 and C_2 are the fitting parameters, we obtain the critical exponents $\eta_E^{(S)}$ which are tabulated in Table I. In practice, we used

two different cutoffs in the fitting: $|\mathbf{q}-\mathbf{Q}|^2 \leq 0.1$ and ≤ 0.5. The fitting for the latter is shown in Fig. 7, and the final quoted errors take into account the uncertainty due to the cutoffs.

Similarly, we also computed the structure factor for the spin operator $S_\sigma(\mathbf{q})$ using Fast Fourier transform while computing the height-height correlation function within the same Monte Carlo simulations. Results are shown in Fig. 8 and the extracted exponents are also tabulated in Table I. Fitting precedure used is exactly the same as that for bond-energy except that we fit $S_\sigma(\mathbf{q})$ to the function $C_1|\mathbf{q}-\mathbf{Q}|^{2(x_\sigma-1)}$ with C_1 and x_σ being the fitting parameters. From Table I, we note that the critical exponents extracted in this way are in good agreement with those obtained from stiffness constant utilizing the interfacial representation, however, the latter yields much better statistical errors by an order of magnitude using the same Monte Carlo simulation data. This clearly demonstates the superiority of the interfacial representation in extracting critical exponents from numerical data. Similar points were made regarding other models, but based on much less extensive simulation data, in Refs. [11] and [13].

Similar fits were attempted for $2S = 6$, yielding $\eta_E^{(S)}(2S=6) = 0.53 \pm 0.41$ and $\eta_\sigma^{(S)}(2S=6) = 0.236 \pm 0.036$. While the statistical error on $\eta_E^{(S)}(2S=6)$ is too large to render the fitting meaningful, the increase in the value of $\eta_\sigma^{(S)}(2S=6)$ when compared with $\eta_\sigma^{(S)}(2S=5)$ is added evidence that $2S=6$ is *not* in the rough phase; if it were still rough at that value of S, we would have expected a continuation of the decreasing trend of $\eta_\sigma^{(S)}$ with S.

As for the cases of $2S = 7$ and 8, the structure factors of both the spin and bond-energy operators show *weaker* than power-law behavior as $\mathbf{q} \to \mathbf{Q}$, as in Figs. 7 and 8, but they increase to a larger value (not seen in these logarithmic plots) right *at* $\mathbf{Q}$. This is indeed consistent with the δ-function singularity. expected if these cases fall into the smooth phase with long-ranged order of the spin and bond-energy operators.

Finally, we consider the uniform magnetization correlation exponent η_M. When $S > 3/2$, it can be predicted (see $\eta_M^{(K)}$ in Table I) that $\eta_M < 2$, implying a divergent (ferromagnetic) susceptibility and a divergent structure factor $S_M(\mathbf{q})$ as $\mathbf{q} \to 0$ Now, due to the linear relation (19) between $\{M(\mathbf{R})\}$ and $\{\sigma(\mathbf{r})\}$, we immediately obtain $S_M(\mathbf{q}) \sim S_\sigma(\mathbf{q})$ near $\mathbf{q} = 0$, just as $S_E(\mathbf{q}) \sim \langle |z(\mathbf{q})|^2 \rangle$ near $\mathbf{q} = \mathbf{Q}$ (see Sec. III E and Eq. (23)) Thus, a singularity at $\mathbf{q} = 0$ is expected in the structure factor of spin operator which is plotted in Fig. 9. From this figure, it appears that only for $2S = 4$, 5, and 6 does $S_M(\mathbf{q})$ show a power-law singularity indicated by a straight line in this log-log plot. This confirms the prediction based on the stiffness constant; however, the numerical values of η_M extracted this way (see Table I) differ considerably from those calculated from the stiffness constant in the case of $2S = 5$ and 6.

It is also apparent from Table I that $\eta_\sigma^{(S)}$ is systematically overestimated as compared with the more accurate value derived from height fluctuations. We suspect that a similar overestimation affected the values of η_σ that were deduced from the finite-size scaling of the susceptibility of the staggered magnetization [15,16] (this obviously measures the same fluctuations seen in $S_\sigma(\mathbf{q})$ near $\mathbf{Q}$.) Those data (also quoted in Ref. [17]) have quoted errors about four times as large as ours for $\eta_\sigma^{(K)}$. Their exponent values are all noticeably larger than the accurate value ($\eta_\sigma^{(K)}$ or η_∞ from Ref. [17]) – becoming *worse* as S grows (for $2S = 4, 5$ the difference is twice their their quoted error.) Clearly the systematic contribution to their errors was underestimated. The transfer-matrix method [17] ought to provide the effective exponent η_σ for spin correlations on length scales comparable to the strip width, and hence is likewise expected to overestimate η_σ; indeed, every η_σ value found in Ref. [17] is slightly larger than our corresponding $\eta_\sigma^{(K)}$ value.

E. Smooth Phase

Which type of flat state is actually selected in the smooth phase? Fig. 10 shows the measured expectation of n_s, the number of zero spins in the spin-1 representation, for $1 \leq 2S \leq 8$. As S grows, it is found that $\langle n_s \rangle$ approaches its maximum allowed value $N_s/3$ as in the $(+,-,0)$ state, rather than zero, as in the $(+,+,-)$ state. Thus, the flat states with half-integer valued $h(\mathbf{R})$ in Fig. 1 are being selected in the smooth phase. Translating back to the spin-S model, this means that spins on two sublattices of the triangular lattice take the extremal values, $+S$ and $-S$ respectively, while spins on the third sublattice remain disordered.

It is perhaps more illuminating to study the distribution of height variables to probe the height fluctuations in the smooth phase. To this end, we also show, in Fig. 10, the histogram of height variable $h(\mathbf{R})$ in the cases of $2S = 2$ and $2S = 8$, which is measured for a *typical* configuration generated in the Monte Carlo simulations. [31]. The broad distribution observed in the case of $2S = 2$ ($S < S_L$) evolves to a narrowly peaked distribution in the case of $2S = 8$ ($S > S_L$). (It decays as $\exp(-\text{const}|h - \langle h \rangle|)$.) This supports the intuitive picture presented in Sec. IV B. Furthermore, the center of this peaked distribution is half-integer valued. (Numerically, the mean is $\langle h \rangle = 0.46$ for the distribution plotted in Fig. 10.) In other words, the locking potential $V(h)$ favors the $(+,0,-)$ type of flat state, in which one sublattice is flippable, rather than the $(+,+,-)$ type of flat state. (See Fig. 1). This kind of flat state was also expected analytically in the limit of large S [29,30].

We have also computed Var(h) for each value of S, in two ways. First, Var(z) is just normalization factors times $\sum_{\mathbf{q}\neq\mathbf{0}}\langle|z(\mathbf{q})|^2\rangle$, which we accumulated throughout the Monte Carlo run, as described earlier in this section; then it can be shown that $Var(h) = Var(z) - \frac{1}{3} + \frac{1}{2}\langle n_s\rangle$ exactly. For $N_s = 72$ this gives Var(h) = 1.06 and 0.20 for $2S = 2$ and $2S = 8$, respectively, showing the contrast of the rough and smooth behavior. Secondly, we can compute Var(h) directly from the histogram (from one snapshot) seen in Fig. 10; this gives respective values 1.1 and 0.15, in satisfactory agreement with the first method.

The exotic "hidden order" phase [17,20] (see Sec. IV B) can be ruled out on the basis of these data: according to Eq. (25) the variance of $h(\mathbf{R})$ should be at least $(3/2)^2 = 2.25$ in the hidden-order phase, while our measurements indicate it is at most only 0.20. Furthermore, for $2S = 7$ and 8, the structure factor $S_\sigma(\mathbf{Q})$ at the zone-corner wave vector $\mathbf{Q}$ (not plotted) was much larger than at nearby $\mathbf{q}$; that direct suggests a δ-function singularity in the thermodynamic limit, i.e., existence of long-ranged spin order in which $\langle s(\mathbf{r})\rangle \neq 0$ on at least two of the sublattices.

Additionally, the spin structure factor $S_\sigma(\mathbf{q})$ near the zone-corner wave vector $\mathbf{Q}$ (Fig. 8) showed a striking curvature in the "smooth" cases $2S = 7$ and 8, quite different from the behavior at smaller S. This makes it plausible that $S_\sigma(\mathbf{q}) \to$ constant, so that spin fluctuations have short-range rather than power-law correlations for $S > S_L$. (It was not emphasized in Ref. [17], but power-law correlations are implied if one takes seriously their measured values $0 < \eta_\sigma < 1/9$ for $2S = 7, 8$.)

We propose, then, that actually $\eta_\sigma = \eta_E = \eta_M = 0$ for $S > S_{c2}$, as in the simplest picture of the smooth phase, and that the observed nonzero values are simply finite-size effects due to the very slow crossover from rough to smooth behavior near a roughening transition (see Sec. VI B, below, for further discussion.)

VI. CONCLUSION AND DISCUSSION

To conclude, in this article, we have investigated the ground-state properties of the antiferromagnetic Ising model of general spin on the triangular lattice by performing Monte Carlo simulations. Utilizing the interfacial representation, we extrapolated the stiffness constants by studying the long-wavelength singularity in the height variables, which in turn lead to straightforward calculation of critical exponents of various operators within the framework of height representation. The results so obtained are further compared with those extracted from a more tranditional method, and demonstrate that the method in terms of height representation method is by far the preferable one for extracting the critical exponents. We also analyzed both the dynamical and static properties of the model in order to map out the phase diagram which consists of three phases with a Kosterlitz-Thouless phase transition at $\frac{3}{2} < S_{KT} < 2$ and a locking phase transition at $\frac{5}{2} < S_L \leq 3$. Even in the smooth state, analysis of the height fluctuations (as in Var(h) was helpful in resolving questions which are made difficult by the strong finite-size effects near the locking transition.

A. Rational exponents?

One of our initial motivations for this study was the possibility of finding rational exponents even for $S > 1/2$. We believe the results in Table I are the first which are accurate enough to rule out this possibility. Indeed, $\eta_\sigma(2S = 4) \approx 3/16$ and $\eta_\sigma(2S = 5) \approx 4/27$, with differences similar to the error (0.001). But *any* random number differs from a rational number with denominator < 30 by the same typical error. The exception is that $\eta_\sigma^{(K)}(2S = 6)$ is quite close to 1/9, but we have given other reasons to be suspicious of this value.

B. What is S_L?

Another intriguing question was whether the critical values $2S_{KT}$ and $2S_L$ are exactly integers. Previous data [17] suggested that $S_L \equiv 3$ exactly, and had large enough errors that $S_{KT} = 3/2$ could not be excluded. Since $\eta_\sigma(S_{KT}) \equiv 1/4$ and $\eta_\sigma(S_L) \equiv 1/9$, this question was answered by the preceding subsection: we find that definitely $S_{KT} < 3/2$. Furthermore, we suspect $S_L < 3$ as concluded in Sec. V C since the effective stiffness at the length scale we access is more than enough to drive the system to the locked phase.

The question of the value of S_L suggests paying closer attention to the behavior of systems near the locking transition. It has been noted previously how the locked phase tends to behave qualitatively like the rough phase in a finite-size system, since the crossover is a very slow function of size. [25] This is consistent with the apparent power-law behaviors observed at $S > S_L$ in previous studies [15,17] and with the tendency of those studies to overestimate the exponents η_σ and η_E (as compared with our more accurate estimates.) This would suggest that, if extensive finite-size corrections were included in our analysis, they would reduce our estimate of S_L a bit further, i.e. we would more definitely conclude that $2S = 6$ is in the locked phase.

Our analysis near the locking transition at S_L suffers from our ignorance of the expected functional form of the critical behavior as a function of $S - S_L$. A study of the roughening transition [32] used the Kosterlitz-Thouless (KT) renormalization group to derive analytic approximations for the total height fluctuation (closely analogous to Var(h) in our problem), which made it possible to

overcome very strong finite-size effects and fit the roughening temperature precisely. Use of KT finite-size corrections was also essential in extracting meaningful numbers from transfer-matrix calculations near the locking transition induced by a magnetic field in Ref. [25]. Thus, a similar adaptation of the KT renormalization group to give expressions for the behavior of $\langle |z(\mathbf{q}|^2 \rangle$, as a function of (small) $|\mathbf{q}|$ and $S - S_L$, or the functional form of $K(S)$ near S_L, could make possible a more conclusive answer as to whether $S_L = 3$ exactly.

C. Possible improved algorithms

Since the long-wavelength behavior in this model (in its rough phase) is purely Gaussian with $z = 2$ (see Sec. V B), the critical slowing down is particularly transparent. It seems feasible to take advantage of the existence of a height representation to develop an acceleration algorithm. For example, it might be possible to extend the cluster algorithms which are known for the $S = 1/2$ triangular Ising antiferromagnet. [33] These are well-defined at $T > 0$, but their effectiveness seems to depend in a hidden fashion on the existence of the height representation when $T \to 0$.

An intriguing alternative approach starts from the observation that at long wavelengths the system obeys Langevin dynamics (see Sec. V B and Ref. [5]). Fourier acceleration [34], a nonlocal algorithm (efficient owing to use of the Fast Fourier Transform algorithm), is known to be effective in such cases. The key is to replace the uncorrelated noise function $\xi(\mathbf{x}, t)$ of Eq. (30) with a new correlated noise function having $\langle |\xi(\mathbf{q}, t)|^2 \rangle \sim 1/|\mathbf{q}|^2$. This might be implemented by first constructing a random function with such correlations, and then updating flippable spins with probabilities determined by that function, in such a fashion as to satisfy detailed balance.

Additionally, it may be possible to analyze transfer-matrices using the height representation. Quite possibly this would yield an order-of-magnitude improvement in the accuracy of the numerical results, for the same size system, similar to the improvement in analysis of Monte Carlo data. The transfer matrix breaks up into sectors corresponding to the step made by $z(\mathbf{r})$ upon following a loop transverse to the strip (across the periodic boundary conditions. Then the stiffness can be extracted directly from the ratio of the dominant eigenvalues of two such sectors; such an analysis is already standard for quasicrystal random tilings, for which the long-wavelength degree of freedom is also an effective interface [35].

ACKNOWLEDGMENTS

C.Z. gratefully acknowledges the support from NSF grant DMR-9419257 at Syracuse University. C.L.H. was supported by NSF grant DMR-9214943.

TABLE I. Stiffness constant and critical exponents. Here $\eta_\sigma^{(K)}$, $\eta_E^{(K)}$ and $\eta_M^{(K)}$ are the estimates for the critical exponents of spin and bond-energy operators calculated from the stiffness constant K as done in Sec. V(C), while $\eta_\sigma^{(S)}$, $\eta_E^{(S)}$, and $\eta_M^{(S)}$ stand for the same critical exponents, but extracted from the singularities of their respective structure factors in Sec. V(D). Estimated errors are also given in the parenthesis.

$2S$	K	$\eta_\sigma^{(K)}$	$\eta_E^{(K)}$	$\eta_M^{(K)}$	$\eta_\sigma^{(S)}$	$\eta_E^{(S)}$	$\eta_M^{(S)}$
1	0.349(0.001)	0.500(0.002)	2.001(0.008)	4.502(0.018)	0.511(0.013)	1.844(0.057)	
2	0.554(0.003)	0.315(0.001)	1.260(0.006)	2.836(0.013)	0.332(0.016)	1.340(0.072)	
3	0.743(0.004)	0.235(0.001)	0.940(0.005)	2.114(0.011)	0.254(0.019)	1.047(0.082)	
4	0.941(0.006)	0.186(0.001)	0.742(0.004)	1.670(0.010)	0.203(0.022)	0.791(0.092)	1.634(0.014)
5	1.188(0.008)	0.147(0.001)	0.588(0.004)	1.322(0.009)	0.180(0.026)	0.504(0.115)	1.560(0.015)
6	1.597(0.015)	0.109(0.001)	0.437(0.004)	0.984(0.009)	0.236(0.036)	0.530(0.410)	1.527(0.016)

* Electronic address: chen@npac.syr.edu

[1] R. Liebmann, *Statistical Physics of Periodically Frustrated Ising Systems*, Springer Lecture Notes on Physics No. 251 (1986).

[2] J. Stephenson, J. Math. Phys. **5**, 1009 (1964); J. Math. Phys. **11**, 413 (1970).

[3] (a). H. W. J. Blöte and H. J. Hilhorst, J. Phys. A **15**, L631 (1982); (b). B. Nienhuis, H.J. Hilhorst, and H.W. Blöte, J. Phys. A **17**, 3559 (1984).

[4] W. Zheng and S. Sachdev, Phys. Rev.B **40**, 2704 (1989); L. S. Levitov, Phys. Rev. Lett. **64**, 92 (1990); S. Sachdev and N. Read, preprint cond-mat/9604134.

[5] C.L. Henley, "Relaxation time for a dimer covering with height representation", preprint cond-mat/9607222 (submitted to J. Stat. Phys., 1996).

[6] C. Zeng, A.A. Middleton and Y. Shapir, "Ground-state roughness of disordered substrate and flux lines in $d = 2$", preprint (submitted to Phys. Rev. Lett., 1996).

[7] D.A. Huse and A.D. Rutenberg, Phys. Rev. B **45**, 7536 (1992).

[8] P. Chandra, P. Coleman, and I. Ritchey, J. Phys. I (France) **3**, 591 (1993).

[9] H. W. J. Blöte and B. Nienhuis, Phys. Rev. Lett. **72**, 1372 (1994)

[10] J. Kondev and C.L. Henley, Phys. Rev. Lett. **73**, 2786 (1994).

[11] J. Kondev and C.L. Henley, Phys. Rev. B **52**, 6628 (1995).

[12] J. Kondev and C.L. Henley, Nuc. Phys. B **464**, 540 (1996).

[13] R. Raghavan, C.L. Henley, and S.L. Arouh, "New two-color dimer models with critical ground states", preprint cond-mat/9606220 (to appear, J. Stat. Phys., 1997).

[14] J. K. Burton and C. L. Henley, "Simulations of a constrained antiferromagnetic Potts model", preprint (to be submitted to J. Phys. A, 1996).

[15] O. Nagai, S. Miyashita and T. Horiguchi, Phys. Rev. B **47**, 202 (1993).

[16] Y. Honda, A. Lipowski, and T. Horiguchi, Phys. Rev. B **52**, 13429 (1995).

[17] A. Lipowski, T. Horiguchi, and D. Lipowska, Phys. Rev. Lett. **74** 3888 (1995).

[18] The limit of $S \to \infty$ is well-defined and has been simulated by Ref. [30] and by Y. Yamada, S. Miyashita, T. Horiguchi, M. Kang, and O. Nagai, J. Mag. Mag. Mater. **140-144**, 1749 (1995). It is interesting as a model which has an infinite number of continuous degrees of freedom (changes of S_z for loose spins), under which the energy is degenerate; in such systems it is expected that a particular average pattern of order is selected when fluctuations are taken into account, but it is nontrivial to compute the selecting terms of free energy, since the potential minimum is flat rather than quadratic as a function of the spins.

[19] S. Miyashita and H. Kawamura, J. Phys. Soc. Jpn. **54**, 3385 (1985); B. Kleine, E. Müller-Hartmann, K. Frahm, and P. Fazekas, Z. Phys. B **87**, 103 (1992); Q. Sheng and C. L. Henley, J. Phys. Cond. Mat. **4**, 2937 (1992). G. Murthy, D. Arovas, and A. Auerbach, preprint (cond-mat/9607217).

[20] A. Lipowski and T. Horiguchi, J. Phys. A **28**, 3371 (1995).

[21] T. Ogawa and Y. Nakajima, Prog. Theor. Phys. (Suppl.) **87**, 90 (1986), independently identified the height representation, but considered the height as defined modulo 6 (so "roughness' could not be clearly defined, and the connection to power-law correlations was not evident.)

[22] Although we only describe the interfacial representation for the spin-1 model, a very similar procedure can be carried out for the original spin-S model straightforwardly. Contrary to what is suggested in Ref. [17], p. 3890, it is also possible to construct $z(\mathbf{r})$ directly from $\{s(\mathbf{r})\}$ for general S, *without* first mapping it to a spin-1/2 or spin-1 model. The prescription is simply to replace $\sigma(\mathbf{r}) \to s(\mathbf{r})/S$ on the right-hand side of (5). The long wavelength height fluctuations would be the same under the new definition; it would be useful only at nonzero temperature, to confirm that excitations have Burgers vector the

[23] L.V. José, L.P. Kadanoff, S.R. Kirkpatrick, and D.R. Nelson, Phys. Rev. B **16**, 1217 (1977).

[24] It had long been noted that the triangular Ising model could be mapped apporoximately to a 6-state clock model model (see E. Domany, M. Schick, J. S. Walker, and R. B. Griffiths, Phys. Rev. B **18**, 2209 (1978), particularly in connection with the effect of adding a second-neighbor ferromagnetic interactionn The height mapping of the *microstates*, is more powerful, in that it shows *every* excitation must correspond to vortex/antivortex pairs; this is important in predicting the $T > 0$ behavior.

[25] H. W. J. Blöte and M. P. Nightengale, Phys. Rev. B **47**, 15046 (1993).

[26] J. Kondev, J. de Gier, and B. Nienhuis, preprint cond-mat/9603170; J. Kondev, to appear *proc. Exactly soluble models in Statistical Mechanics"* (March 1996, Northeastern University), cond-mat/9607181.

[27] G. H. Wannier, Phys. Rev. **79**, 357 (1950).

[28] P. Chandra, P. Coleman, and L. B. Ioffe, Phys. Rev. B **49**, 12897 (1994) used a height representation to understand the phase diagram of another triangular antiferromagnet; the behavior is reminiscent of the $S = \infty$ limit in our system (discussed in footnote [18]).

[29] T. Horiguchi, O. Nagai, and S. Miyashita, J. Phys. Soc. Jpn. **60**, 1513 (1991).

[30] T. Horiguchi, O. Nagai, S. Miyashita, Y. Miyatake, and Y. Seo J. Phys. Soc. Jpn. **61**, 3114 (1992).

[31] A plaquette has half-integer-valued $h(\mathbf{R})$ if and only if it has a zero spin at exactly one corner (Fig. 1). From this it follows that the total weight of the half-integer bars in the in the histogram is $3\langle n_s\rangle/N_s$; this clarifies the relation between the upper and lower panels of Fig. 10.

[32] H. G. Evertz, M. Hasenbusch, M. Marcu, and K. Pinn, Physica A **199**, 31 (1993).

[33] P. D. Coddington and L. Han, Phys. Rev. B **50**, 3058 (1994); G. M. Zhang and C. Z. Yang, Phys. Rev. B **50**, 12546 (1994).

[34] G. G. Batrouni, G. R. Katz, A. S. Kronfeld, G. P. Lepage,

B. Svetitsky, and K. G. Wilson, Phys. Rev. D **32**, 2736 (1985).
[35] C. L. Henley, J. Phys. A **21**, 1649 (1988); W. Li, H. Park, and M. Widom, J. Stat. Phys. **66**,1 (1992).

FIG. 1. Twelve flat states of the ground-state ensemble. Each flat state is simply specified by its spins on three sublattices A, B, and C of the triangular lattice since all spins on same sublattice take the same value. The height variable $h(\mathbf{R})$ defined at the center of an elementary triangle according to Eq. (4), which is uniform for each of these twelve states, is also shown. Note that $h(\mathbf{R}) \to h(\mathbf{R}) + 6$ results in identical spin configurations. The three nearest-neighbor vectors $\mathbf{e}_1$, $\mathbf{e}_2$ and $\mathbf{e}_3$ defined in Eq. (1) are also displayed.

FIG. 2. Auto-correlation function of Fourier components of the height variables $z(\mathbf{q})$ for $2S = 1$. Only those corresponding to the five smallest $|\mathbf{q}|^2$ are shown where we have averaged over data points with the same value of $|\mathbf{q}|^2$. The discrete $\mathbf{q}$-vectors comes about because of the periodic boundary condition used for the Monte Carlo simulation cell which consists of 72×72 spins. The solid lines in the figure are the fittings discussed in Sec. IV(B) to extrapolate the relaxation time $\tau_{\mathbf{q}}$ where we have used a cutoff in time $t \leq 10$ measured in the unit of MSC.

FIG. 3. Relaxation time $\tau_{\mathbf{q}}$ as a function of $\mathbf{q}^{-2}$ for $2S = 1, ..., 8$. The solid lines are the fittings for cases of $2S = 1, ..., 6$ from bottom to top (see Sec. V(B)). The dotted lines in the insert are only the guide for eyes where data for $2S = 6, 7$ and 8 are displayed from top to bottom.

FIG. 4. Structure factor $S_h(\mathbf{q})$ of height variables. We show in the main figure the inverse of the structure factor as a function of $\mathbf{q}^2$ for $2S = 1$. The lower envelope of the data corresponds to $q_y = 0$. As an insert to the figure, we plot all the lower bounds for $2S = 1, 2, ..., 8$ which go from bottom to top. Solid lines in the insert are only the guide for eyes. Note that $\mathbf{q}^2 = 17.5459...$ corresponds to the corner of the first Brillouin zone, i.e., $\mathbf{q} = \mathbf{Q} \equiv \frac{4\pi}{3}(1, 0)$.

FIG. 5. Scaling of $\langle |z(\mathbf{q})|^2 \rangle^{-1}$ as a function of $\mathbf{q}^2$. We have averaged data points of the same magnitude of $\mathbf{q}$-vector in each case of $2S = 1, 2, ..., 8$ obtained for system sizes $L = 36, 48$, and 72. Note the error bars are smaller than the symbol size. Solid lines are fits using a cutoff $\mathbf{q}^2 \leq 0.5$ discussed in Sec. V(C). Dotted lines are only guides for the eye.

FIG. 6. Extrapolation of stiffness constants. We show $[\mathbf{q}^2 \langle |z(\mathbf{q})|^2 \rangle]^{-1}$ vs. $\mathbf{q}^2$ as log-linear plot for $2S = 1, 2, ..., 6$. Note that we have performed an average over data points with the same magnitude of $\mathbf{q}$-vector for each case of $2S$. Solid lines are the linear fitting discussed in Sec. V C in order to extract the stiffness constant which is given by the intercept of the fitting. Also note that the fittings shown are performed with a cutoff $\mathbf{q}^2 \leq 0.5$. Fittings with other cutoffs are discussed in the text.

FIG. 7. Structure factor $S_E(\mathbf{q})$ of the bond-energy operator near the zone corner $\mathbf{Q}$. Data points are averaged results over those with the same $|\mathbf{q} - \mathbf{Q}|^2$ value for each case of $2S = 1, 2, ..., 8$. Note that data points for each $2S$ have been shifted upwards by 0.5 with respect to their counterpart for $2S - 1$ in order to disentangle the data. Solid lines are the fittings discussed in Sec. V(D) to extract the critical exponent η_E of the bond-energy operator. Dotted lines are only to guide the eye.

FIG. 8. Structure factor $S_\sigma(\mathbf{q})$ of the spin operator near the zone corner $\mathbf{Q}$. Data points are averaged results over those with the same $|\mathbf{q} - \mathbf{Q}|^2$ value for each case of $2S = 1, 2, ..., 8$. Note that data points for each $2S$ are moved downwards by 0.1 with respect to their counterpart for $2S - 1$ in order to disentangle the data. Solid lines are the fittings discussed in Sec. V(D) to extract the critical exponent η_σ of the spin operator. Dotted lines are only to guide the eye.

FIG. 9. Structure factor $S_M(\mathbf{q})$ of the spin operator near the zone center $\mathbf{q} \to 0$. Data points are averaged results over those with the same $|\mathbf{q}|^2$ value for each case of $2S = 1, 2, ..., 8$. Note that data points for each $2S$ are moved upwards by 0.15 with respect to their counterpart for $2S - 1$ in order to disentangle the data. Solid lines are the fittings discussed in Sec. V(D) to extract the critical exponent η_M of the uniform magnetization operator. Dotted lines are only to guide the eye.

FIG. 10. Height distribution and ensemble average of the number of free spins n_s, from one snapshot for each S value. On the top panel, we show the histograms of the height variables $h(\mathbf{R})$ for $2S = 2$ and $2S = 8$. On the bottom panel, n_s is displayed as a function of $2S$. Note that the maximum allowed value for $\langle n_s \rangle$ is $N_s/3$ where N_s denotes the total number of spins in the simulation cell.

Fig. 2 - Zeng and Henley

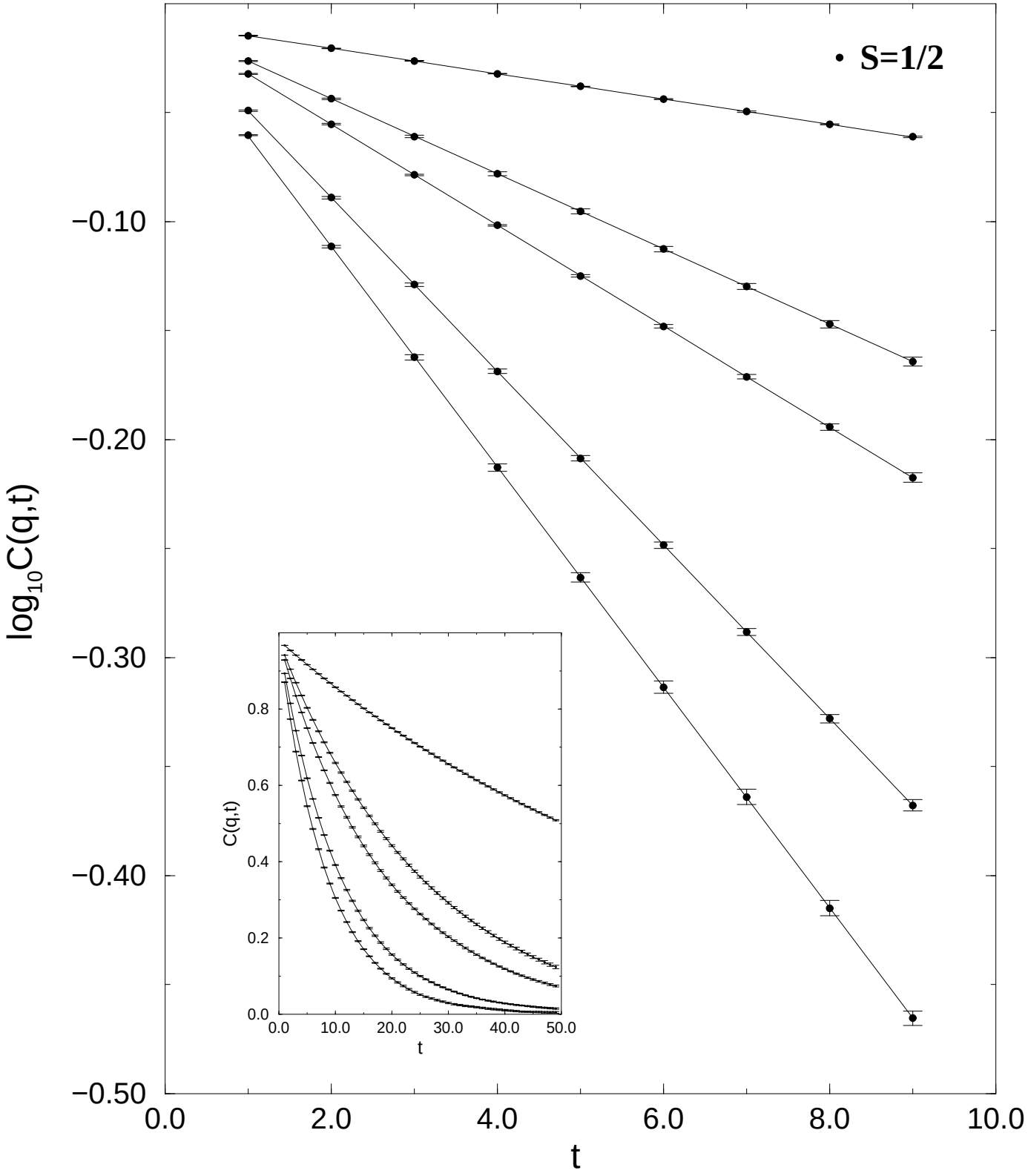

Fig. 4 - Zeng and Henley

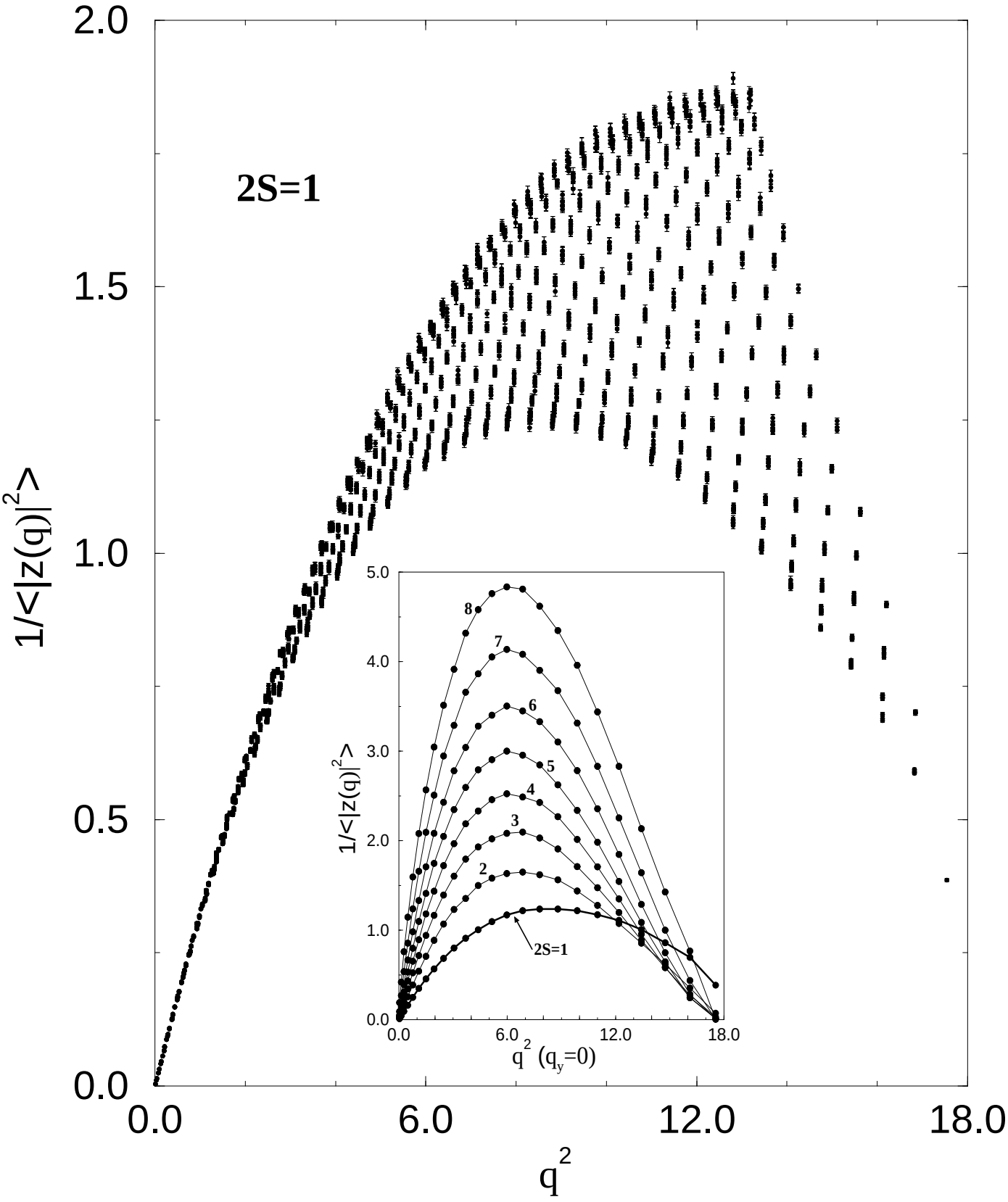

Fig. 1 - Zeng and Henley

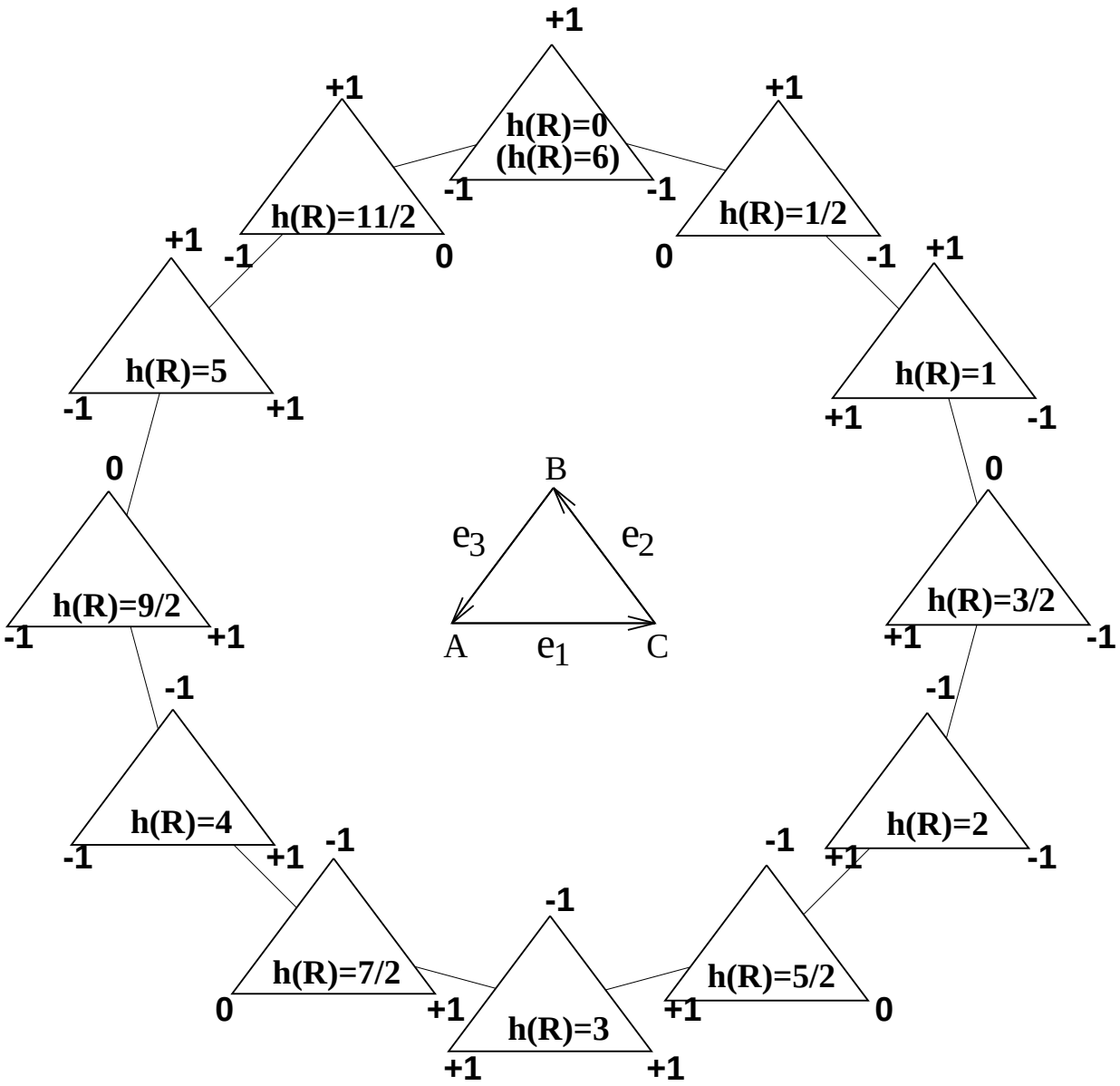

Fig. 10 - Zeng and Henley

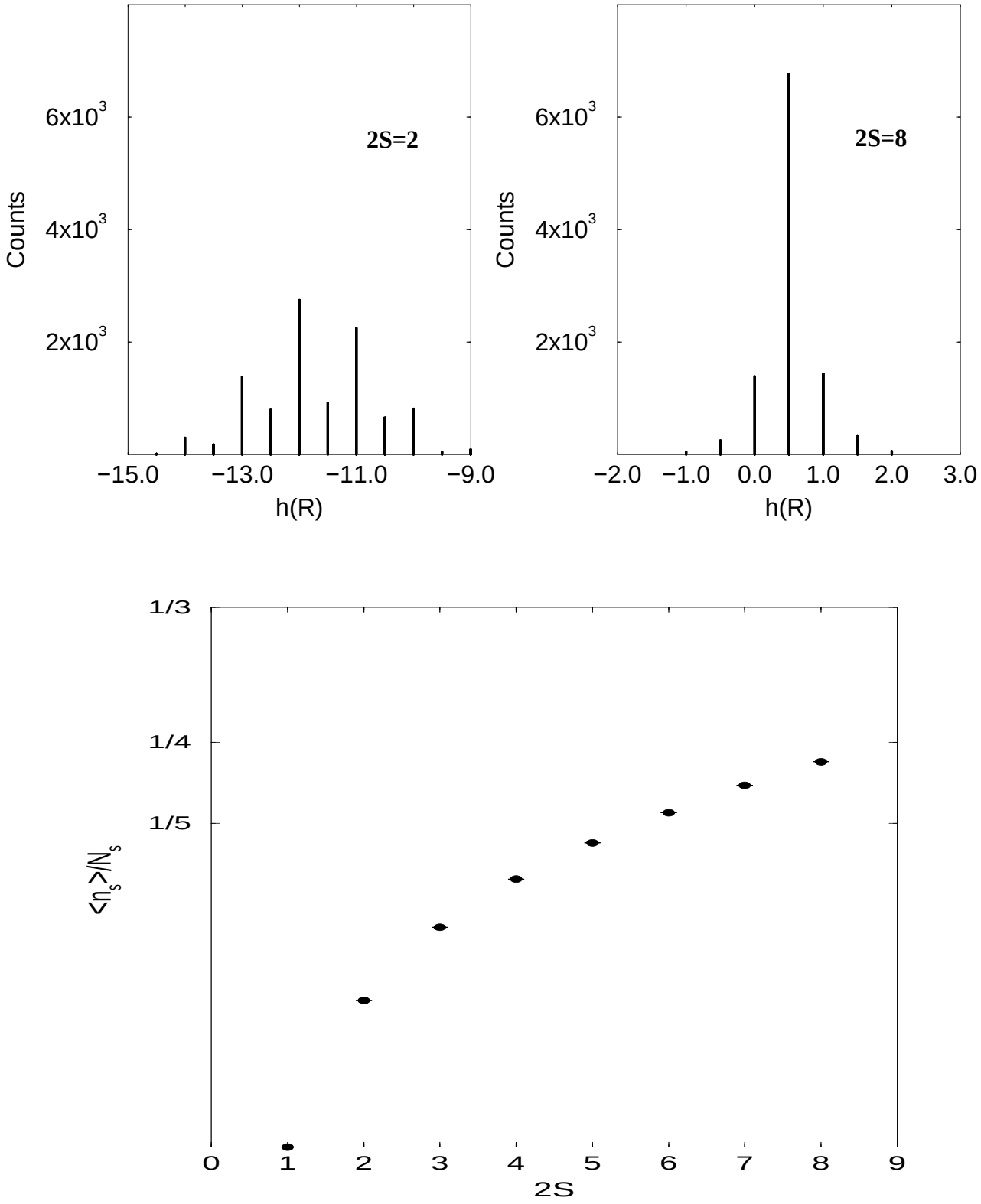

Fig. 5 - Zeng and Henley

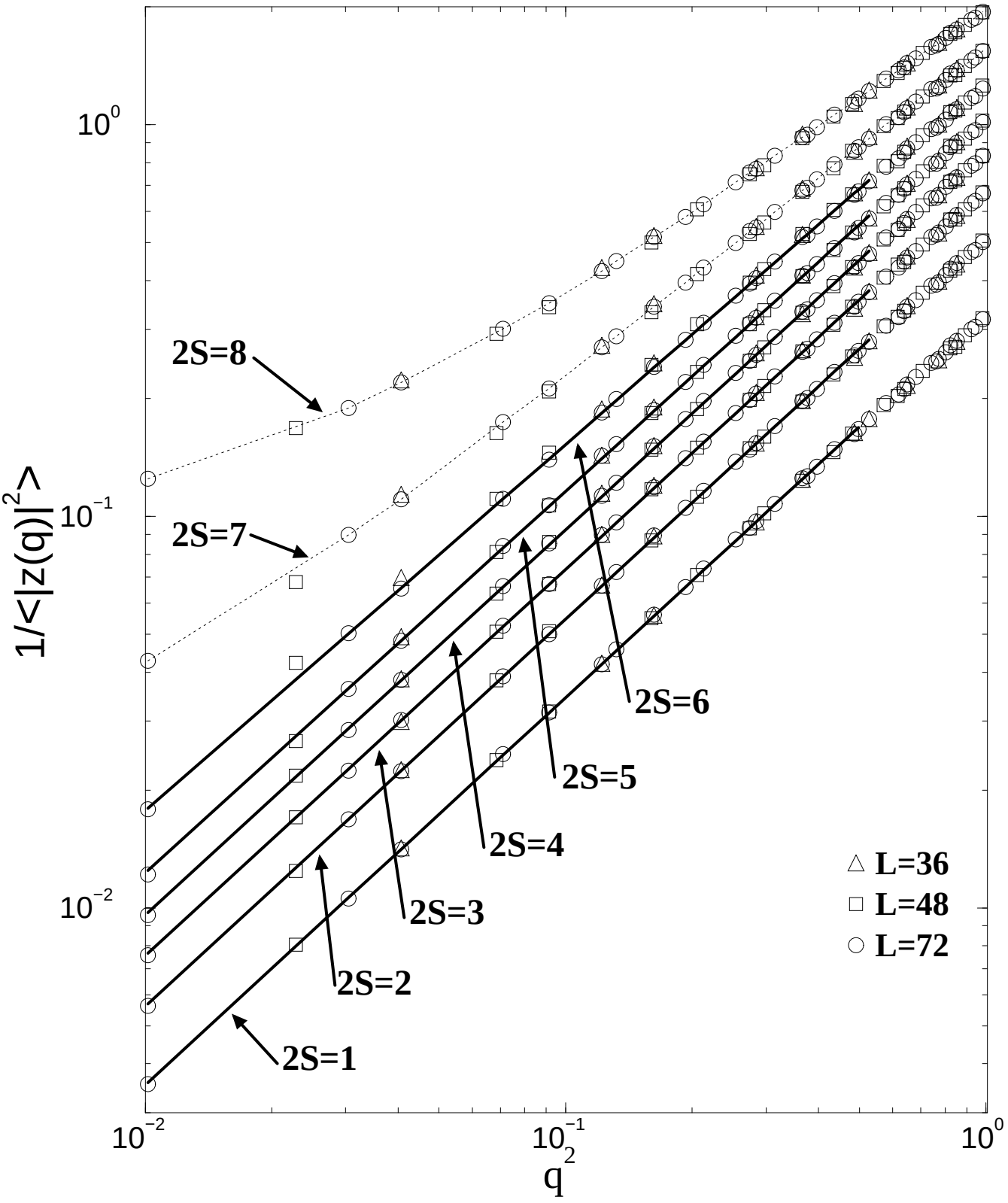

Fig. 6 - Zeng and Henley

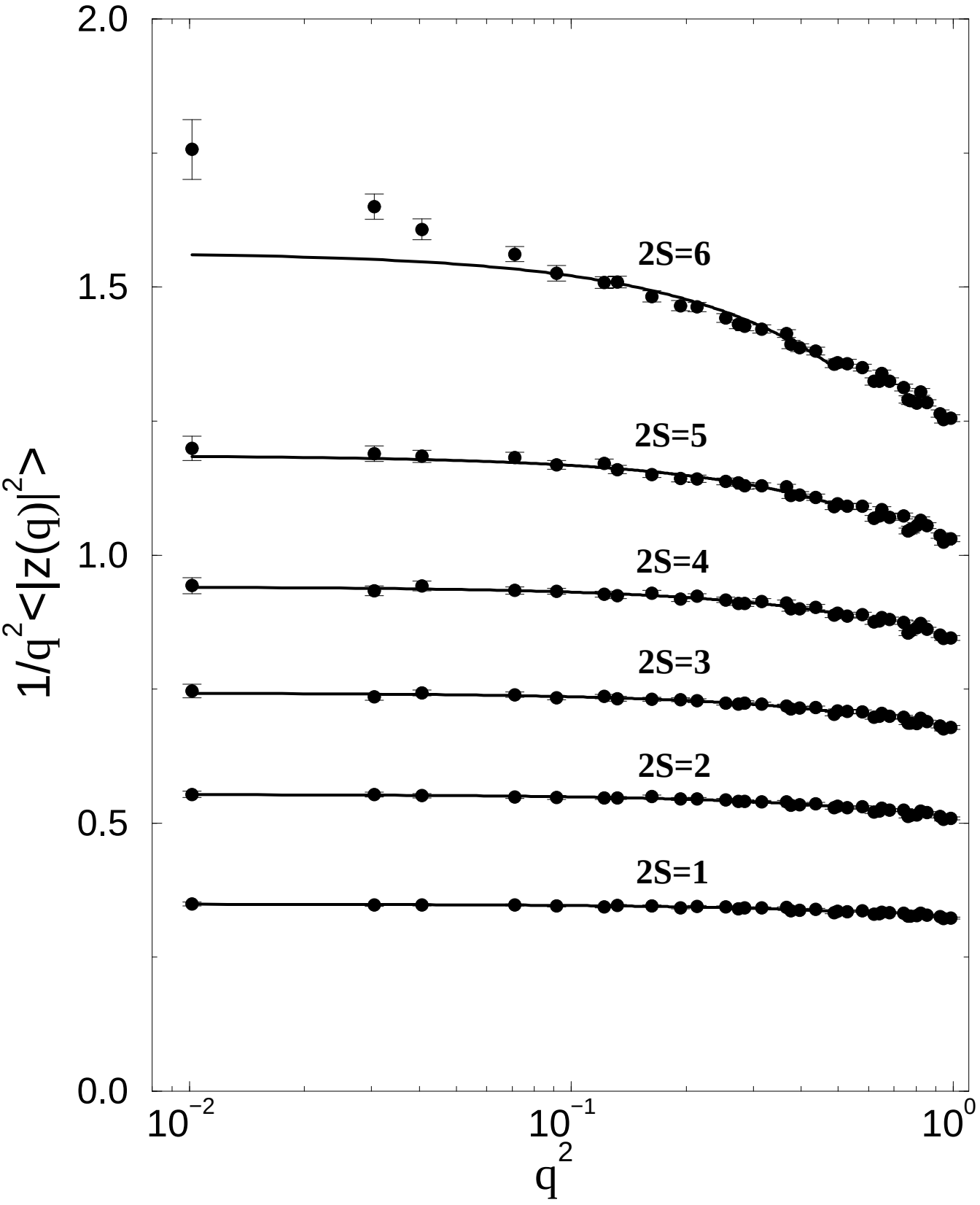

Fig. 9 - Zeng and Henley

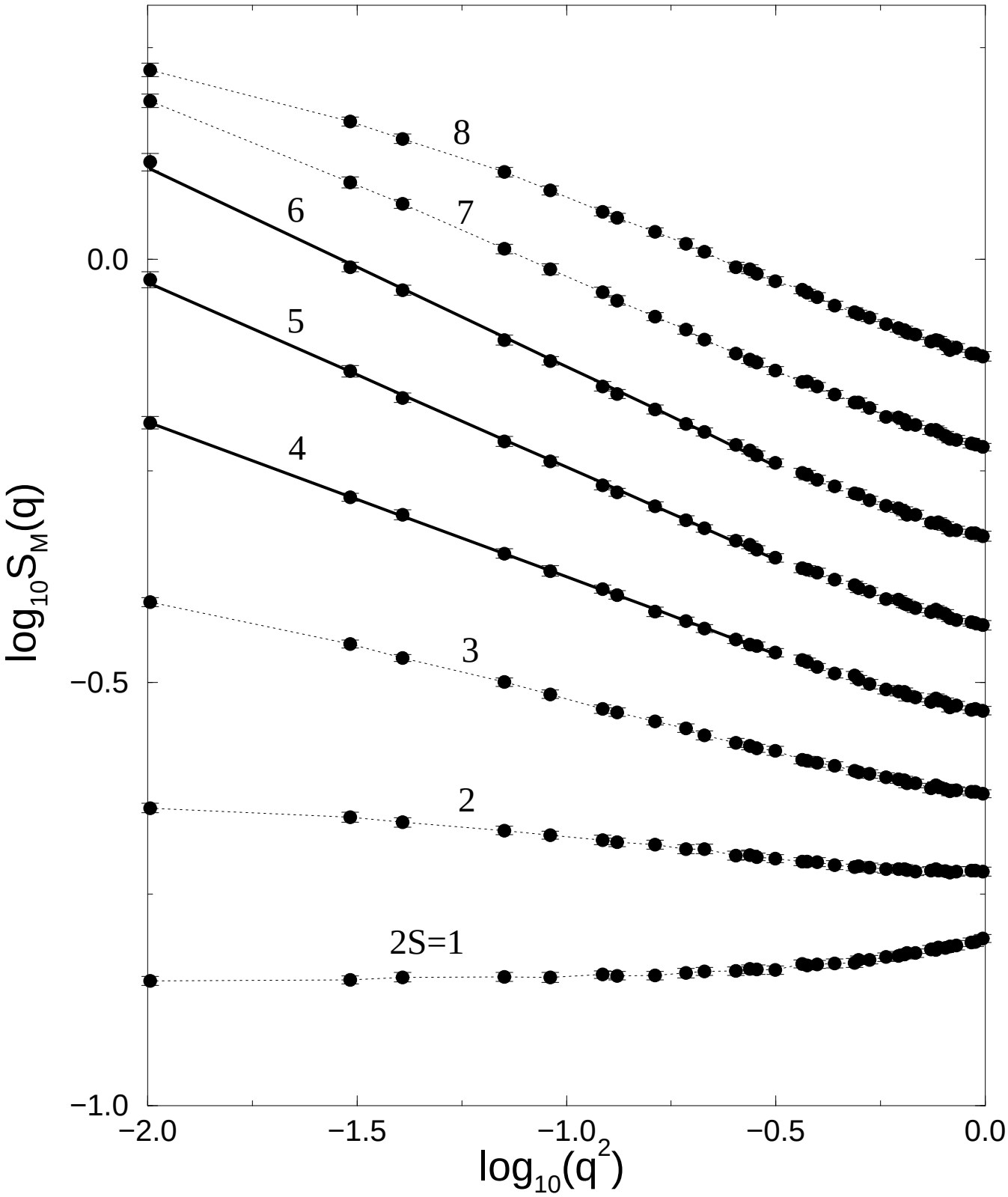

Fig. 8 - Zeng and Henley

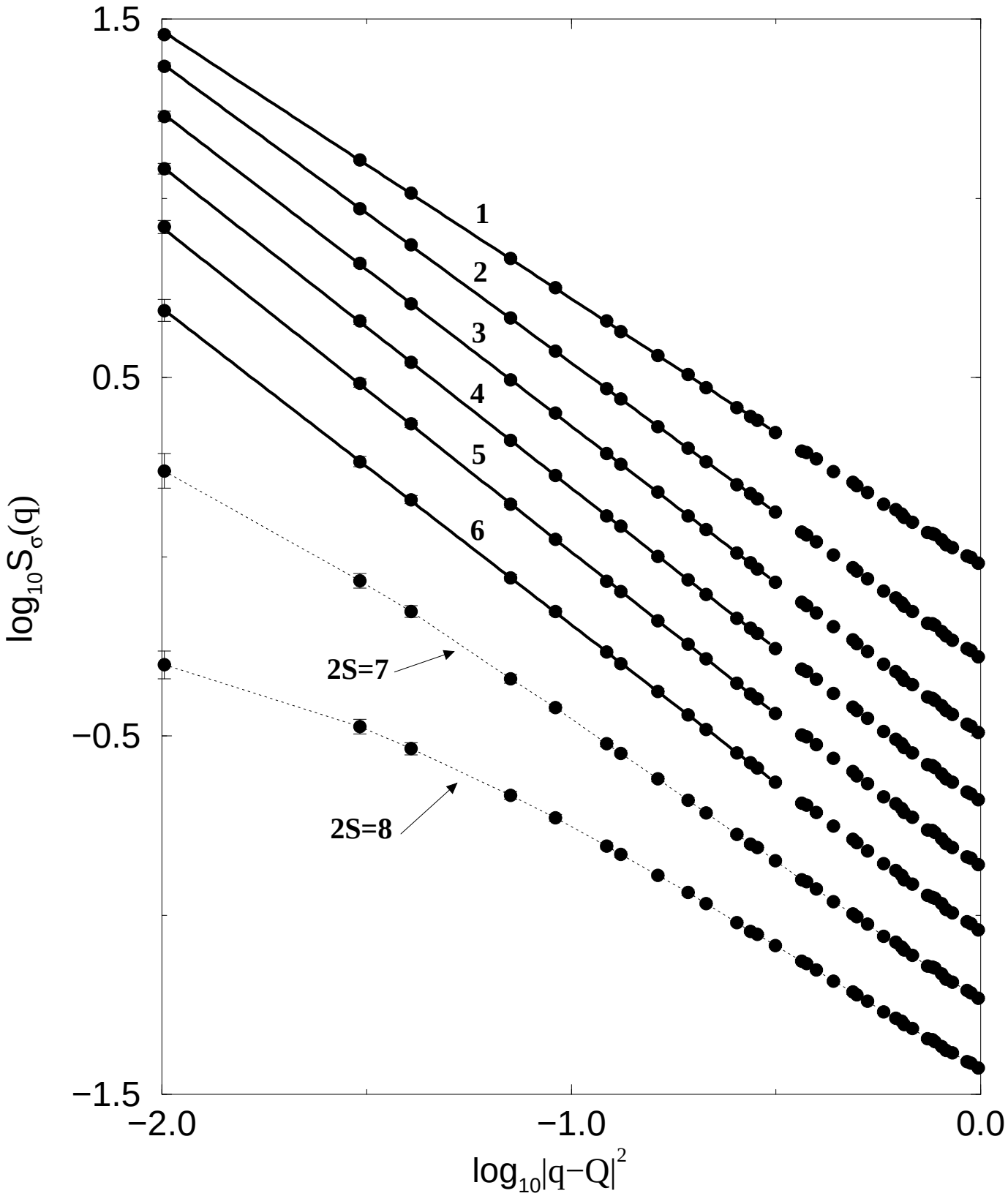

Fig. 3 - Zeng and Henley

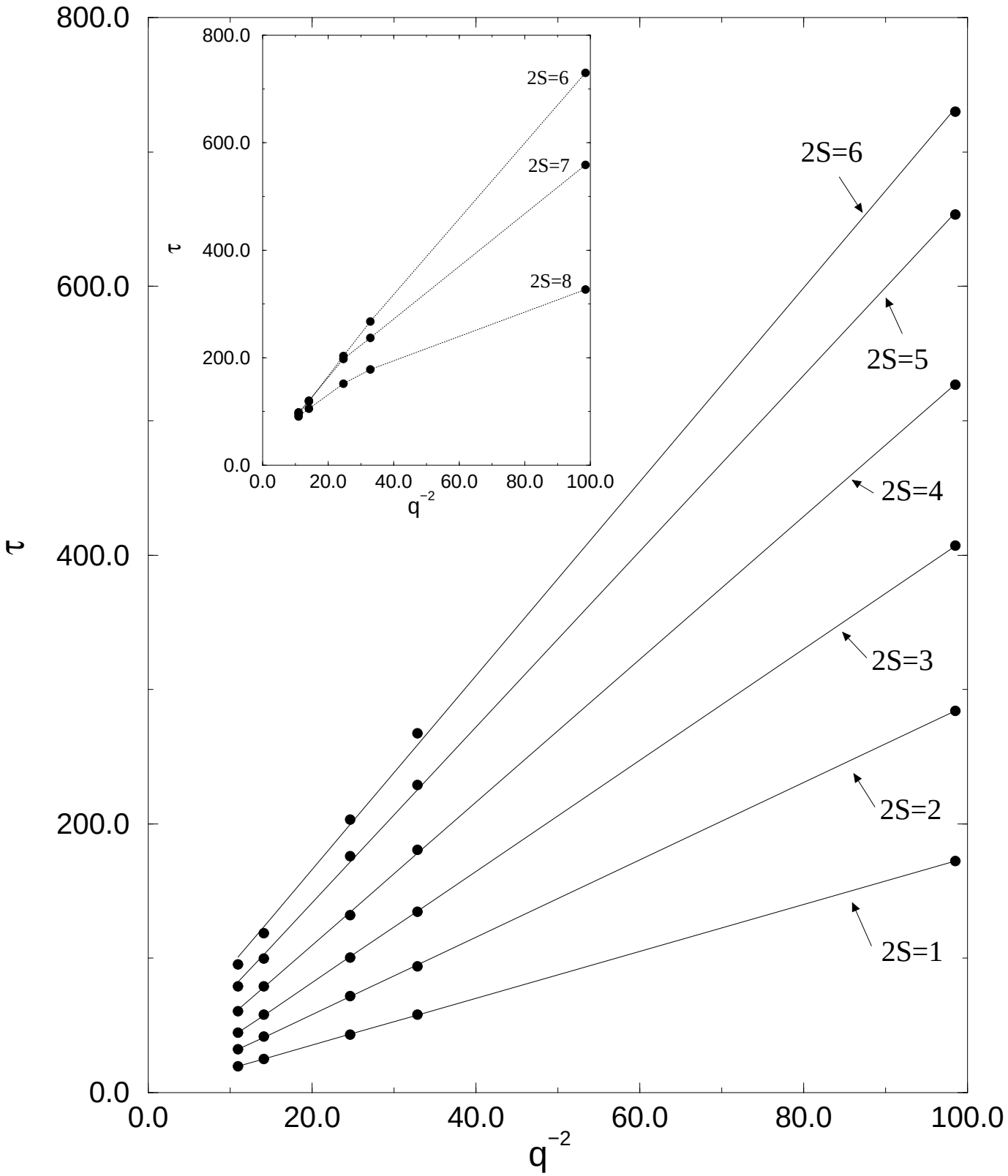

Fig. 7 - Zeng and Henley